Clays and Clay Minerals, Vol. 48, No. 6, 610–631, 2000.

REACTION MECHANISMS OF SMECTITE ILLITIZATION ASSOCIATED WITH HYDROTHERMAL ALTERATION FROM PONZA ISLAND, ITALY

ROBERT F. YLAGAN,[1,†] STEPHEN P. ALTANER,[1] AND ANTONIO POZZUOLI[2]

[1]University of Illinois, Department of Geology, 1301 W. Green, Urbana, Illinois 61801 USA
[2]Università degli Studi di Napoli 'Federico II', Dipartimento di Geofisica e Vulcanologia, Largo S. Marcellino 10 80138 Napoli, Italy

Abstract—A hydrothermally altered rhyolitic hyaloclastite from Ponza island, Italy, has four alteration zones with unique clay assemblages: (1) a non-pervasive argillic zone characterized by smectite; (2) a propylitic zone with interstratified illite-smectite (I-S) containing 10–85% illite (I); (3) a silicic zone composed of I-S with ≥90% I and pure illite; and (4) a sericitic zone with I-S ranging from 66% I to pure illite. Atomic force microscopy reveals abrupt changes in particle morphology with illitization, including initial changes from anhedral plates to laths and then to euhedral plates and hexagonal plates. I-S particles progressively thicken with illitization and mean particle area (basal plane) remains constant from pure smectite to I-S with 80% I. However, particle area increases from 90 to 100% illite. Computer modeling of I-S structural forms indicates octahedral cation ordering progressively changes from *cis*-vacant smectite to interstratified *cis*- and *trans*-vacant I-S, and then to *trans*-vacant illite. In addition, polytypes progressively change from $1M_d$ to $1M$, and then to $2M_1$ illite. Electron-microprobe and X-ray fluoresence analyses show that I-S chemistry progressively changes during illitization, evolving toward a phengitic composition with ~0.89 fixed interlayer K^+ per $O_{10}(OH)_2$. Octahedral Mg^{2+} shows little change with illitization, varying from 0.3 to 0.5 cations per $O_{10}(OH)_2$. The layer charge of smectite is ~0.38 equivalents per $O_{10}(OH)_2$.

On the basis of abrupt changes in morphology and progressive changes in polytype and chemistry, smectite illitization on Ponza involved a dissolution and recrystallization mechanism with multiple stages of nucleation and crystal growth. In this multi-step model, temperature of alteration provided the major control for the layer composition, polytype, and morphology of I-S crystallites. Other factors that may play a secondary role include: K^+ availability, water-rock ratio, and permeability. Alternatively, the mechanism of I-S and illite formation at Ponza and other hydrothermal environments may occur by direct precipitation of I-S crystallites from rhyolite glass and may not involve progressive reactions of smectite precursors.

Key Words—Atomic Force Microscopy, Chemical Analysis, Illite, Polytype, Smectite, XRD.

INTRODUCTION

Numerous studies (see review by Altaner and Ylagan, 1997) of smectite illitization have proposed various reaction mechanisms which can be grouped into two general categories: solid-state transformation (SST) and dissolution and crystallization (DC). An SST mechanism involves the gradual and topotactic replacement of smectite by illite. This mechanism features gradual changes in Reichweite ordering, similar polytypes of the smectite and illite crystals, and illite crystals with a similar size and shape as the smectite precursor (Barronet, 1992). Pollard (1971) proposed a mechanism where Al and Si diffuse through the interlayer, followed by tetrahedral-sheet distortions as Al replaces Si. Others studies suggest an SST mechanism but do not propose specific models (Hower, 1981; Hunziker *et al.*, 1986; Inoue *et al.*, 1990; Lindgreen *et al.*, 1991).

DC mechanisms involve complete dissolution of smectite followed by crystallization of illite as a separate grain. DC mechanisms feature abrupt changes in Reichweite ordering, polytype, and morphology (Barronet, 1992). On the basis of mineralogic and transmission electron microscopy (TEM) evidence, several DC mechanisms have been proposed for illitization (Nadeau *et al.*, 1984, 1985; Yau *et al.*, 1987; Inoue *et al.*, 1987; Eberl and Środoń, 1988). According to Inoue *et al.* (1987), anhedral smectite crystals become unstable, dissolve, and recrystallize to form thin euhedral laths, some of which dissolve and crystallize to form larger euhedral illite laths and hexagons. Whitney and Velde (1993) proposed a DC model with several stages including smectite dissolution, nucleation of small illite crystals onto smectite templates, and coalescence and growth of illite crystals. Eberl and Środoń (1988) and Inoue *et al.* (1988) concluded that illite recrystallization is controlled by an Ostwald ripening mechanism whereby the smallest crystallites dissolve and reprecipitate onto larger crystallites to minimize the surface free energy. Ahn and Peacor (1986) presented a reaction mechanism intermediate between SST and DC where smectite dissolves and illite replaces the parent smectite.

In summary, some studies favor the DC mechanism (Nadeau *et al.*, 1985), others favor Ostwald ripening

† Present address: ExxonMobil Upstream Research Co., P.O. Box 2189, Houston, Texas 77252-2189 USA.

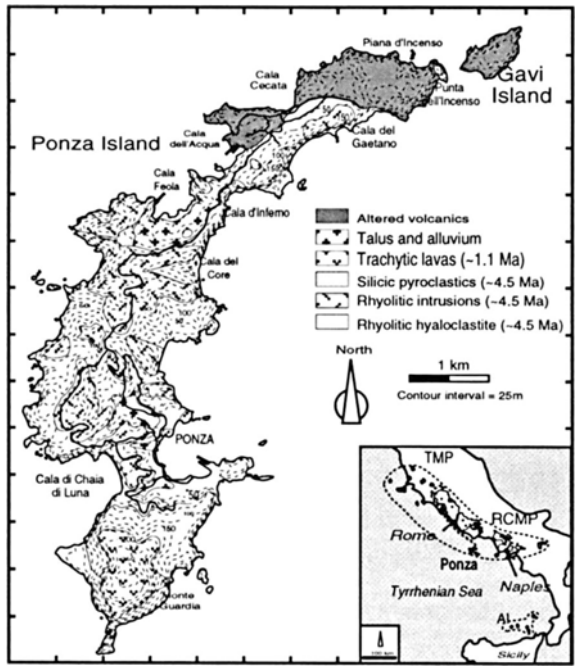

Figure 1. Geologic map of Ponza and Gavi islands (Modified from Carmassi *et al.*, 1983). Inset depicts a regional map of Italy showing the major volcanic provinces. (Modified from Turi *et al.*, 1991). Tuscan magmatic province (TMP) ages are from Ferrara and Tonarini (1985), Fornaseri (1985), and Ferrara *et al.* (1988); Roman comagmatic province (RCMP) ages are from Capaldi *et al.* (1985).

(Eberl *et al.*, 1990), and still others favor an SST mechanism (Hunziker *et al.*, 1986; Lindgreen *et al.*, 1991; Clauer *et al.*, 1995). Several studies emphasize that different mechanisms may apply in different geologic environments: an SST or local DC mechanism describing illitization in shale and bentonite (Inoue *et al.*, 1990; Ahn and Peacor, 1986; Li *et al.*, 1997) and a DC or Ostwald ripening mechanism in hydrothermal settings (Yau *et al.*, 1987; Inoue *et al.*, 1988; Christidis, 1995). Based on crystallite shapes and size distributions, Lanson *et al.* (1998) proposed different pathways for illitization in different sedimentary basins. In addition, other studies suggest the reaction mechanism changes from SST where illite-smectite (I-S) exhibits Reichweite, R = 0 order to DC where I-S has R ≥ 1 order (Drits, 1987; Whitney and Northrop, 1988). Inoue *et al.* (1987) suggested a three-step process of K^+ fixation, followed by DC, and then followed by Ostwald ripening.

It is important in geologic studies to understand the reaction mechanism of smectite illitization because, if illitization occurs by an SST mechanism, then geochemical analyses of I-S minerals (*e.g.*, K/Ar ages and $\delta^{18}O$ values) represent an average over a broad range of environmental conditions. However, if illitization occurs by a DC mechanism, then these data represent the diagenetic conditions during the final stage of illitization. The objective of this paper is to characterize the reaction mechanism of smectite illitization in a natural setting of hydrothermal alteration.

GEOLOGIC SETTING

Regional geology

Ponza island is on the western coast of Italy in the Tyrrhenian Sea along with numerous volcanic islands

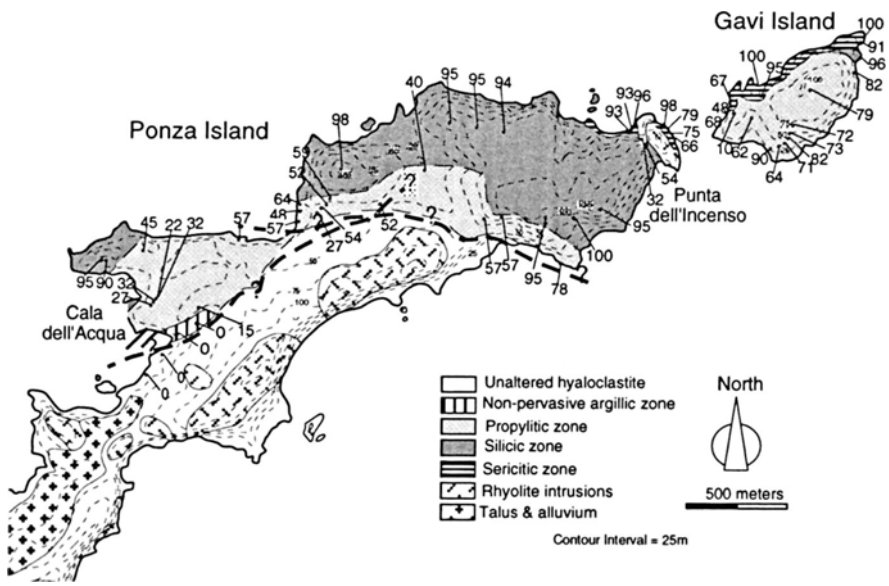

Figure 2. Map of northern Ponza and Gavi indicating sample locations, % Illite in I-S value, and the distribution of the alteration zones. Heavy dashed lines with "?" indicate possible faults (Ylagan *et al.*, 1996).

https://doi.org/10.1346/CCMN.2000.0480603 Published online by Cambridge University Press

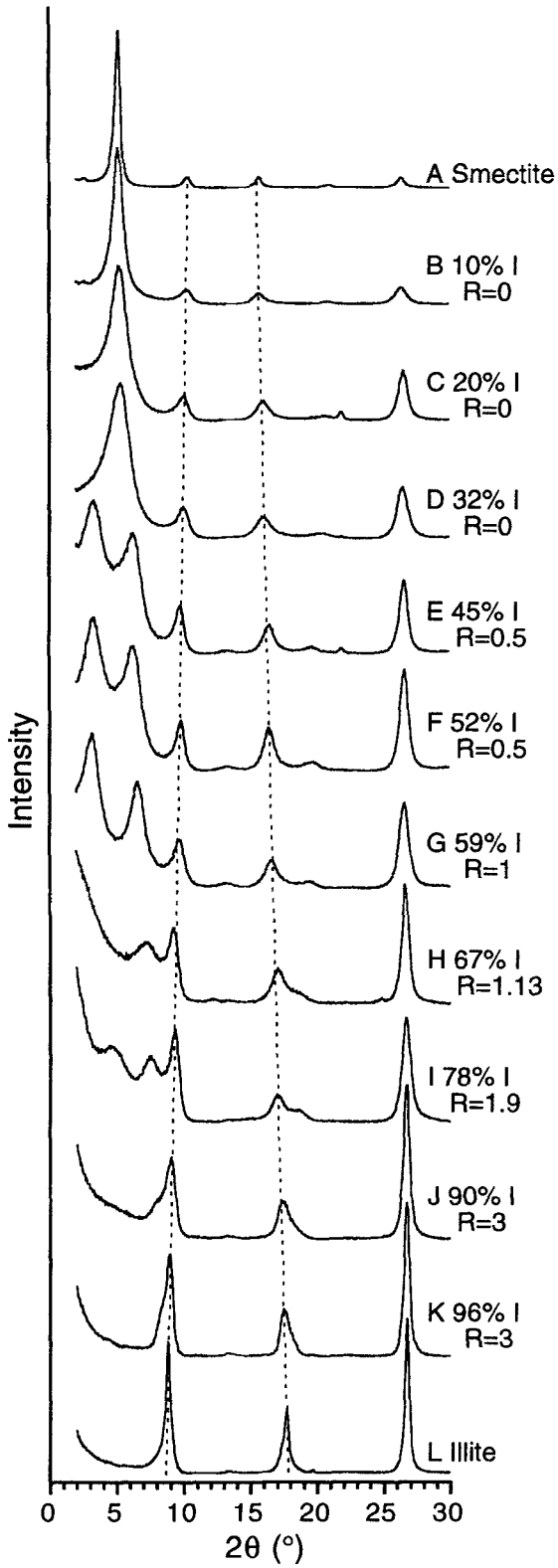

Figure 3. XRD patterns of oriented aggregates of ethylene-glycolated I-S from Ponza and Gavi. % I and R values were determined from best-fit calculated patterns using NEWMOD. Dashed lines indicate diagnostic peak migrations observed during smectite illitization. (A) 93-6-8C, (B) 93-6-10C, (C) 94-6-3M, (D) 94-6-11C, (E) 94-6-3T, (F) 93-6-8Q, (G) 93-6-9Q, (H) 94-6-16C, (I) 94-6-16Q, (J) 93-6-8N, (K) 94-6-16R, and (L) 93-6-10A.

including Palmarola, Ischia, Procida, Stromboli, and Vulcano. Dewey (1988) summarized the tectonic framework for this complex region. The volcanic centers have been classified into two major volcanic provinces on the basis of geochemistry and age (Figure 1, inset). In the north, silica-saturated magmas formed between 7.0–2.5 Ma and are characterized by rhyolite, rhyodacite, and quartz-latite. These magmas comprise the Tuscan Magmatic Province (TMP) (Ferrara and Tonarini, 1985; Fornaseri, 1985; Ferrara *et al.*, 1988; Taylor and Turi, 1976; Peccerillo *et al.*, 1987; Beccaluva *et al.*, 1989; Poli, 1992). In the south, potassic, silica-undersaturated magmas formed <1.5 Ma and are characterized by phonolite, trachyte, and latite. They comprise the Roman-Campanian Magmatic Province (RCMP) (Capaldi *et al.*, 1985; Turi and Taylor, 1976; Hawkesworth and Vollmer, 1979; Rogers *et al.*, 1985; Taylor *et al.*, 1987; Civetta *et al.*, 1989). Calc-alkaline volcanics, located in the Aeolian islands, are derived from NW subduction along the Calabrian arc.

Geologic setting of Ponza

The geologic history of Ponza island (Figure 1) involves two stages of volcanism and alteration of the rocks from the first volcanic stage, although the timing and origin of the alteration are not established (Lombardi and Mattias, 1981). The first volcanic stage involved emplacement of massive dikes and a thick, highly brecciated, rhyolitic hyaloclastite which crop out over most of Ponza and Gavi (Pichler, 1965; Barberi *et al.*, 1967). The hyaloclastite formed at 4.5 Ma by submarine eruption of silicic lavas, which brecciated due to rapid cooling (Pichler, 1965; Barberi *et al.*, 1967; Carmassi *et al.*, 1983). Carmassi *et al.* (1983) proposed that the hyaloclastite and the dikes formed contemporaneously at 4.5 Ma. In this model, the feeder dikes were insulated from contact with seawater, allowing the interior to cool more slowly. Later studies showed that the hyaloclastite and dikes have similar chemical compositions (Savelli, 1987; Marino, 1992) and ages (Savelli, 1983, 1987). Yamagishi and Dimroth (1985) proposed a similar model for the origin of silicic dikes associated with rhyolitic hyaloclastites in Hokkaido, Japan. The second stage of volcanism (1.1 Ma), concentrated in southern Ponza, is characterized by subaerial trachytic eruptions including surge deposits, tuff cones, pyroclastic flows, and lava flows.

Early studies on the Ponza bentonite indicate that smectite is commonly the dominant mineral present

https://doi.org/10.1346/CCMN.2000.0480603 Published online by Cambridge University Press

Table 1. Junction probabilities and R values that describe interlayer ordering in I-S from Ponza. P_I = proportion of illite interlayers expressed as a fraction, P_{I-I} = probability of an illite interlayer to follow a given sequence of one illite interlayer, P_{II-I} = probability of an illite interlayer to follow a given sequence of two illite interlayers, and P_{III-I} = probability of an illite interlayer to follow a given sequence of three illite interlayers.

Sample	Alteration zone	Size fraction (μm)	R	P_I	P_{I-I}	P_{II-I}	P_{III-I}
93-6-8C	Argillic	<0.5	0	0	0	0	0
93-6-8F	Argillic	<0.5	0	0	0	0	0
93-6-10C	Argillic	<0.1	0	0.10	0.10	0.10	0.10
94-6-11A	Propylitic	<0.05	0	0.15	0.15	0.15	0.15
94-6-3M	Propylitic	<0.05	0	0.20	0.20	0.20	0.20
94-6-3J	Propylitic	<0.1	0	0.22	0.22	0.22	0.22
94-6-4C	Propylitic	<0.1	0	0.27	0.27	0.27	0.27
93-6-8M	Propylitic	<0.05	0	0.27	0.27	0.27	0.27
94-6-11C	Propylitic	<0.1	0	0.32	0.32	0.32	0.32
94-6-3N	Propylitic	<0.1	0	0.32	0.32	0.32	0.32
94-6-4G	Propylitic	<0.1	0	0.40	0.40	0.40	0.40
93-6-16B	Propylitic	<0.1	0.5	0.44	0.08	0.08	0.08
94-6-3T	Propylitic	<0.1	0.5	0.45	0.11	0.11	0.11
94-6-16A	Propylitic	<0.1	0.5	0.48	0.20	0.20	0.20
93-6-9O	Propylitic	<0.1	0.4	0.52	0.34	0.34	0.34
93-6-8Q	Propylitic	<0.1	0.5	0.52	0.30	0.30	0.30
94-6-4L	Propylitic	<0.1	0.8	0.54	0.23	0.23	0.23
93-6-9N	Propylitic	<0.1	0.8	0.54	0.23	0.23	0.23
93-6-8T	Propylitic	<0.1	0.35	0.57	0.46	0.46	0.46
93-6-8S	Propylitic	<0.1	0.78	0.57	0.41	0.41	0.41
94-6-2A	Propylitic	<0.1	0.8	0.57	0.31	0.31	0.31
94-6-4A	Propylitic	<0.1	0.5	0.58	0.43	0.43	0.43
93-6-9Q	Propylitic	<0.1	1	0.59	0.31	0.31	0.31
93-6-10B	Propylitic	<0.1	1.15	0.62	0.39	0.24	0.24
93-6-9H	Propylitic	<0.1	1.15	0.62	0.39	0.24	0.24
94-6-4B	Propylitic	<0.1	0.8	0.64	0.48	0.48	0.48
93-6-9G	Propylitic	<0.1	1.15	0.64	0.47	0.33	0.33
94-6-5D	Propylitic	<0.1	0.8	0.66	0.52	0.52	0.52
93-6-9F	Propylitic	<0.1	1.35	0.71	0.59	0.49	0.49
93-6-9C	Propylitic	<0.1	1.36	0.72	0.61	0.52	0.52
93-6-9D	Propylitic	<0.1	1.54	0.73	0.63	0.51	0.51
94-6-16Q	Propylitic	<0.1	1.9	0.78	0.72	0.62	0.62
94-6-16J	Propylitic	<0.1	2	0.82	0.78	0.72	0.72
93-6-9E	Propylitic	<0.1	2	0.82	0.78	0.72	0.72
93-6-8N	Silicic	<0.1	2.5	0.82	0.78	0.72	0.66
93-6-8N	Silicic	<0.5	3	0.90	0.89	0.88	0.86
93-6-10G	Silicic	<0.1	3	0.91	0.90	0.89	0.88
93-6-8O	Silicic	<0.1	3	0.95	0.95	0.94	0.94
93-6-10G	Silicic	<0.5	3	0.96	0.96	0.96	0.95
93-6-8W	Silicic	<0.1	3	1	1	1	1
93-6-9L I	Sericitic	<0.1	1	0.63	0.41	0.41	0.41
93-6-9J	Sericitic	<0.1	1	0.66	0.48	0.48	0.48
94-6-16C	Sericitic	<0.1	1.13	0.67	0.51	0.45	0.45
93-6-9L II	Sericitic	<0.5	1	0.75	0.67	0.67	0.67
93-6-9L I	Sericitic	<0.5	1.5	0.79	0.73	0.69	0.69
94-6-16F	Sericitic	<0.5	3	0.91	0.90	0.89	0.88
93-6-10A	Sericitic	<0.1	3	0.92	0.91	0.90	0.89
94-6-16S	Sericitic	<0.5	3	0.93	0.92	0.92	0.91
94-6-16T	Sericitic	<0.5	3	0.93	0.92	0.92	0.91
94-6-16R	Sericitic	<0.5	3	0.96	0.96	0.96	0.95
93-6-9M	Sericitic	<0.5	3	0.97	0.97	0.97	0.97
93-6-10A	Sericitic	<0.5	3	1	1	1	1
94-6-16D	Sericitic	<0.5	3	1	1	1	1

(Lupino, 1954; Güven and Grim, 1972; Grim and Güven, 1978; Lombardi and Mattias, 1981; Pozzuoli, 1988; Passaglia *et al.*, 1995). However, Ylagan *et al.* (1996) indicate that the outcrop mineralogy consists of I-S, illite, opal-C, mordenite, kaolinite, and various sulfide (pyrite, chalcopyrite, sphalerite, and galena) and sulfate minerals. Ylagan *et al.* (1996) characterized four alteration zones based on authigenic mineralogy and field textures: an argillic, a propylitic, a silicic, and a sericitic zone (Figure 2). Smectite has a

https://doi.org/10.1346/CCMN.2000.0480603 Published online by Cambridge University Press

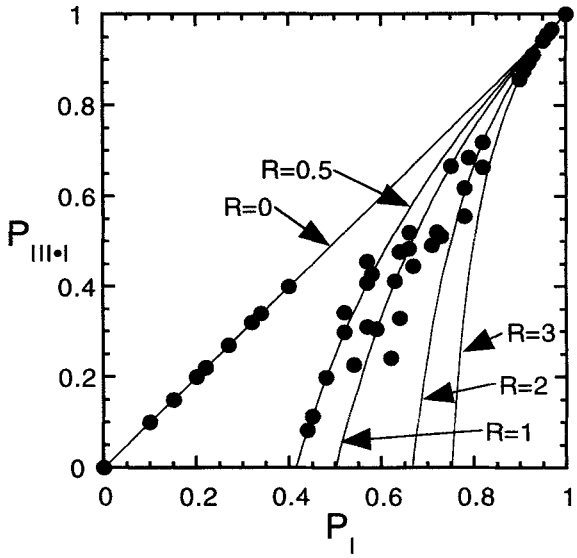

Figure 4. Junction probability diagram for I-S from Ponza and Gavi. P_I = proportion of illite interlayers, P_{III-I} = probability of an illite interlayer to follow a given sequence of three illite interlayers. Labeled lines represent pathways for various Reichweite ordering schemes.

ribbon-like morphology on the basis of transmission electron microscopy (Güven and Grim, 1972; Grim and Güven, 1978). Illitic clays are found in outcrop samples along the extreme northern portion of Ponza and on the neighboring islands of Gavi and Zannone (Lombardi and Mattias, 1981). Pozzuoli (1992) estimated alteration temperatures ranged from 127 to 368°C. However, Ylagan (1996) used oxygen-isotope and fluid-inclusion results to constrain alteration temperatures from 50 to 225°C. Although Passaglia *et al.* (1995) suggested that alteration occurred in an open hydrologic system where meteoric waters reacted with the hyaloclastite under a high geothermal gradient, Ylagan (1996) concluded the bentonite formed from hydrothermal processes involving seawater.

METHODS

X-ray diffraction

Fifty-three samples were collected from the four alteration zones on Ponza. In general, samples from the argillic, silicic, and sericitic zones were purified by isolating the <0.5-μm size fraction, whereas samples from the propylitic zone required the <0.1 or <0.05-μm size fraction to remove fine-grained opal-C and mordenite. Although different size fractions were ob-

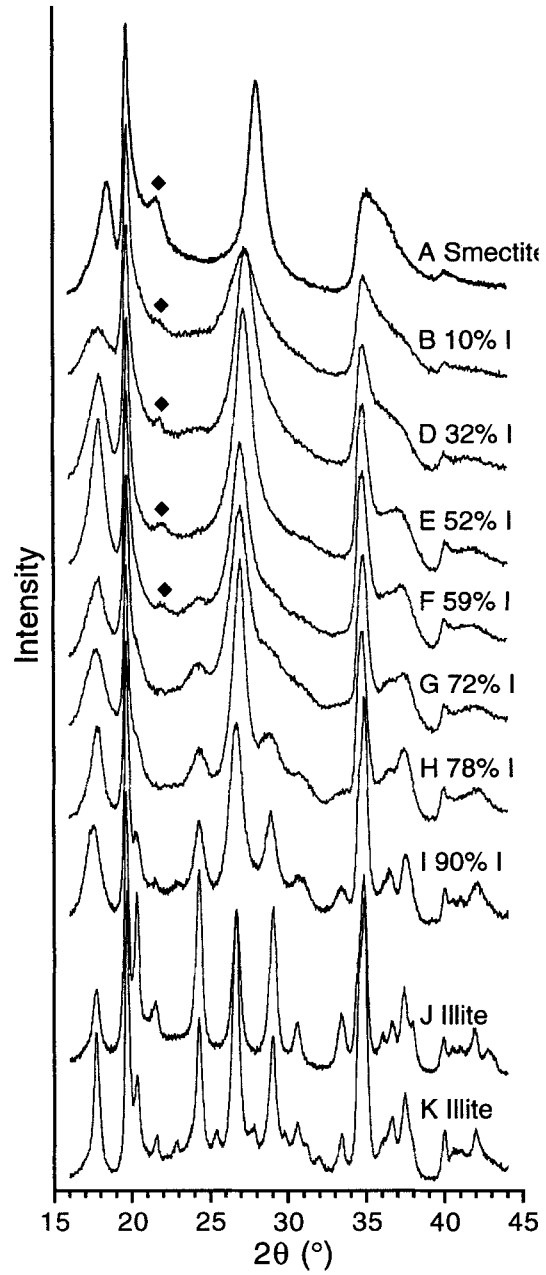

Figure 5. XRD patterns of randomly oriented I-S from Ponza and Gavi. (A)–(J) are samples from the argillic, propylitic, and silicic zones, and (K)–(R) are samples from the sericitic zone. (◆) = opal-CT or opal-C. (A) 93-6-8C, (B) 93-6-10C, (C) 94-6-4C, (D) 94-6-11C, (E) 93-6-8Q, (F) 93-6-9Q, (G) 93-6-9C, (H) 94-6-16Q, (I) 93-6-8N, (J) 93-6-8W, and (K) 93-6-10A.

→

Figure 6. Comparison of XRD patterns calculated using WILDFIRE with experimental patterns of randomly oriented samples of I-S. Table 2 lists all parameters used in calculations. All labeled reflections denote 1*M* peaks except for those with *, which are $2M_1$ peaks. (◆) = opal-CT or opal-C, (●) = authigenic K-rich feldspar. (A) 93-6-8C, (B) 94-6-11C, (C) 93-6-8Q, (D) 93-6-9Q, (E) 93-6-9C, (F) 93-6-9L1, (G) 93-6-8N, and (H) 93-6-10A.

https://doi.org/10.1346/CCMN.2000.0480603 Published online by Cambridge University Press

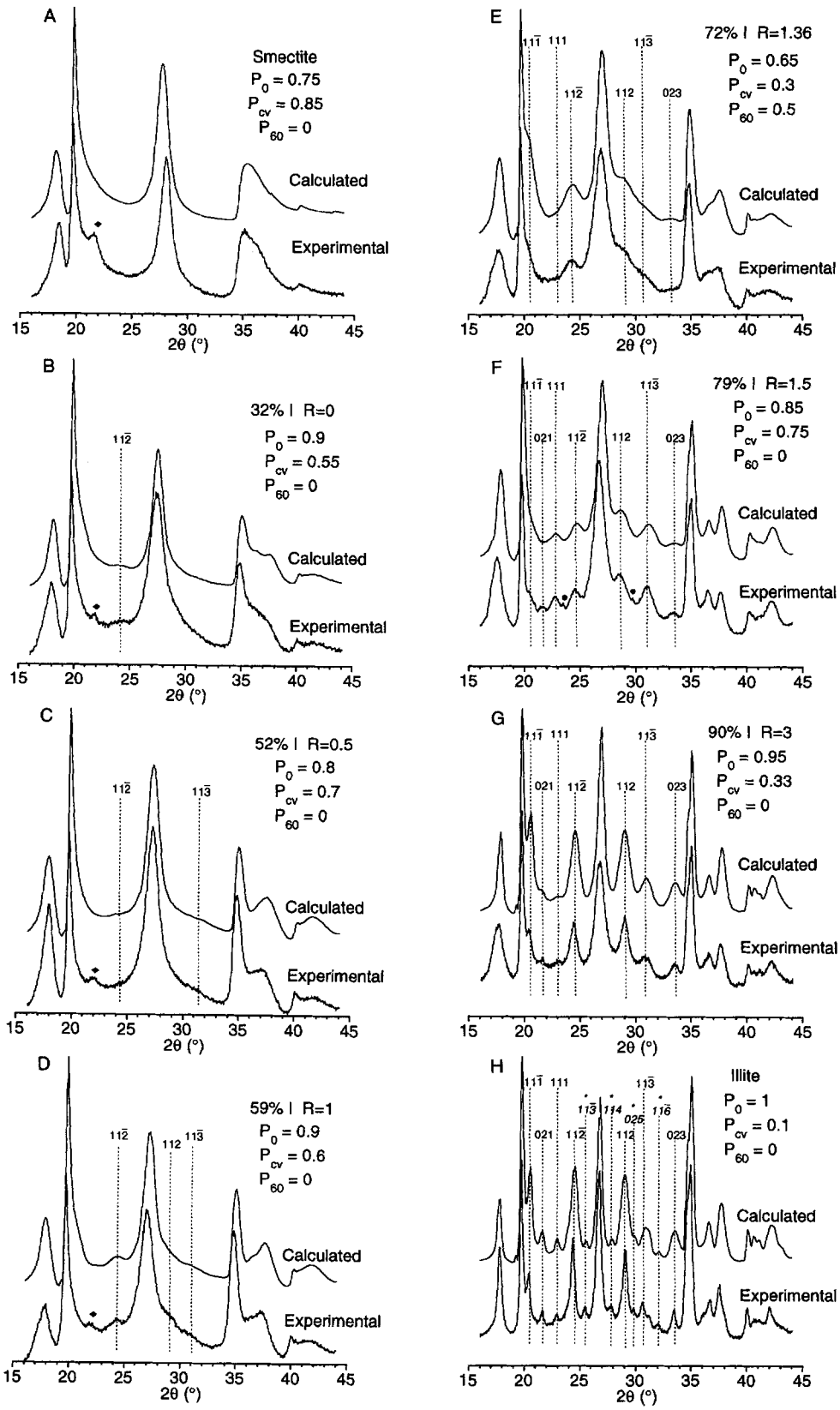

https://doi.org/10.1346/CCMN.2000.0480603 Published online by Cambridge University Press

tained to achieve purity, we believe that size fractionation did not significantly bias any results. Size fractions were obtained by centrifugation and concentrated by vacuum suction onto a Millipore filter. Oriented clay aggregates were transferred onto glass slides for X-ray diffraction (XRD), using a Siemens D-500 diffractometer. XRD patterns were collected from 2–30 °2θ (at 2.5° per min) after air-drying and ethylene-glycol solvation. Ethylene glycol-solvated patterns were modeled using NEWMOD (Reynolds, 1985) to determine the Reichweite ordering and illite content in I-S. Junction probabilities, which are statistical parameters that describe layer ordering, were calculated using equations in Reynolds (1980). Twenty-five samples that ranged from pure smectite to pure illite were selected for further geochemical and mineralogic analysis. A minimum of 2.5 g of each sample was purified, dialyzed to remove salts, and freeze-dried to create a stock powder that was used for all analyses described in this study. Trace amounts of opal-CT or opal-C (≤5 wt. %) were detected by XRD in some clay mineral separates. However, most samples contained only I-S minerals, based on random-powder XRD.

Freeze-drying produces clay separates with a low degree of preferred orientation that are ideal for three-dimensional structural analysis. For each sample, ~300 mg of freeze-dried powder were heated at 250°C for 1 h, side-packed into an Al-holder, and diffraction patterns collected in a dry atmosphere (flushed with N_2 gas) from 16 to 44 °2θ. To improve the signal-to-noise ratio, scan speeds were extremely slow with a step size of 0.04 °2θ and count times of 60 s/step. Each XRD pattern was modeled using the computer program WILDFIRE (Reynolds, 1993a, 1993b) to determine abundance of *cis*-vacant (*cv*) and *trans*-vacant (*tv*) sites and rotational disorder (Tsipursky and Drits, 1984; Drits *et al.*, 1984; Reynolds and Thomson, 1993).

Chemical analysis

To evaluate the reliability, effects of surface roughness, and porosity of electron microprobe (EMP) analysis of I-S clay minerals, 12 untreated I-S powders that ranged from pure smectite to pure illite were analyzed by EMP and compared with results from X-ray fluorescence (XRF) spectroscopy. In addition, 24 Sr-saturated samples were also analyzed by EMP to constrain exchangeable-cation and octahedral-sheet chemistry. I-S samples were continuously shaken for 24 h in a 0.1 M $SrCl_2$ solution, and then centrifuged. The solution was decanted and new solution was added. This process was repeated four times, and samples were then dialyzed to remove any excess $SrCl_2$ and freeze-dried. All samples were prepared for EMP analysis by pressing 10 mg of dialyzed, freeze-dried powder (unexchanged or Sr-saturated) into a 3-mm pellet. Pellets were carbon coated, and analyzed with a Cameca SX-50 microprobe equipped with four wavelength-dis-

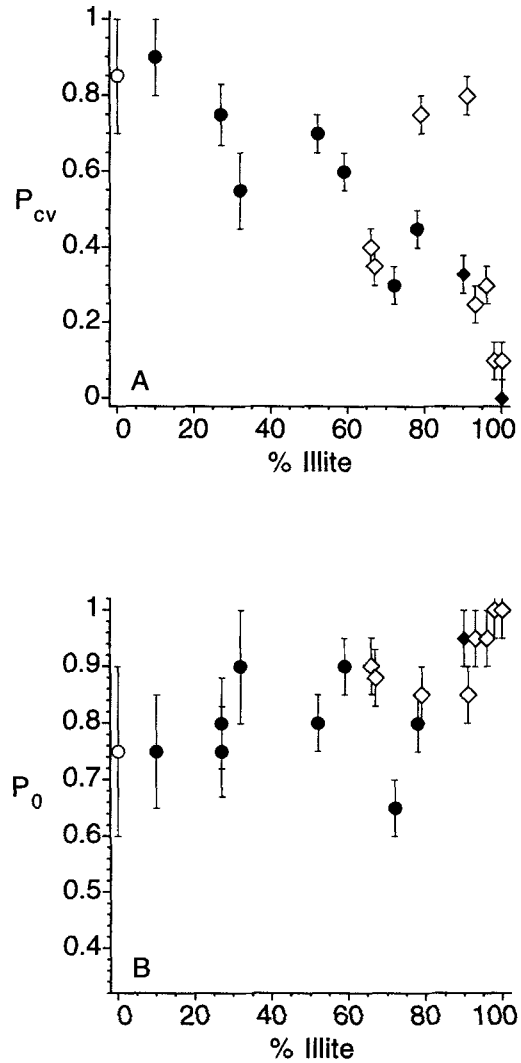

Figure 7. (A) P_{cv} *vs.* % I for I-S from Ponza and Gavi. (B) P_0 *vs.* % I for I-S from Ponza and Gavi. (○) = argillic-zone samples, (●) = propylitic-zone samples, (◆) = silicic-zone samples, and (◇) = sericitic-zone samples. Error bars represent range of best-fit calculated patterns determined by trial and error.

→

Figure 8. Chemistry of structural formulae for Sr-saturated I-S from Ponza and Gavi *vs.* % I in I-S. (A) exchangeable Sr, (B) fixed interlayer K, (C) tetrahedral Si, (D) total layer charge, (E) tetrahedral charge, (F) octahedral charge, (G) octahedral Al, (H) octahedral Fe, and (I) octahedral Mg. See Figure 7 for symbol definitions.

https://doi.org/10.1346/CCMN.2000.0480603 Published online by Cambridge University Press

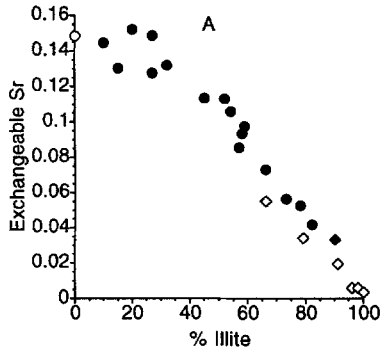

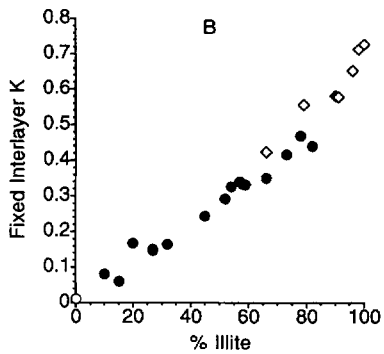

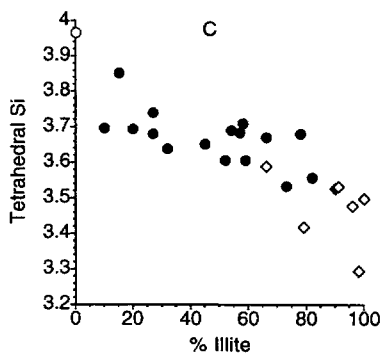

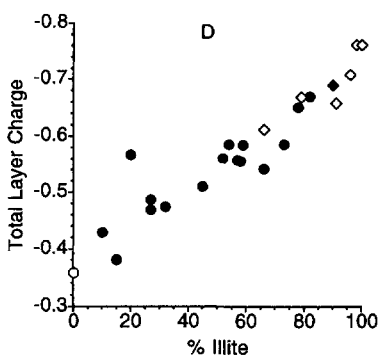

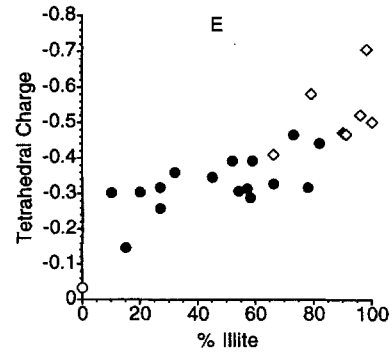

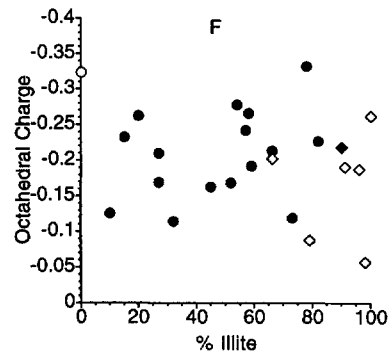

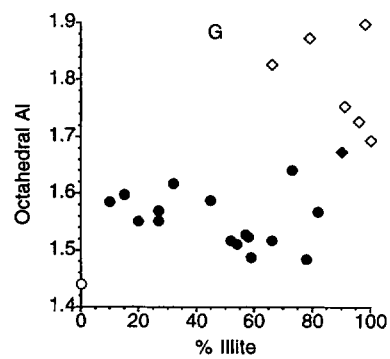

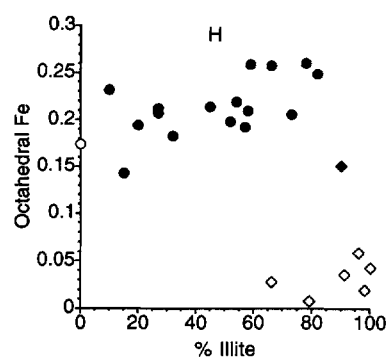

https://doi.org/10.1346/CCMN.2000.0480603 Published online by Cambridge University Press

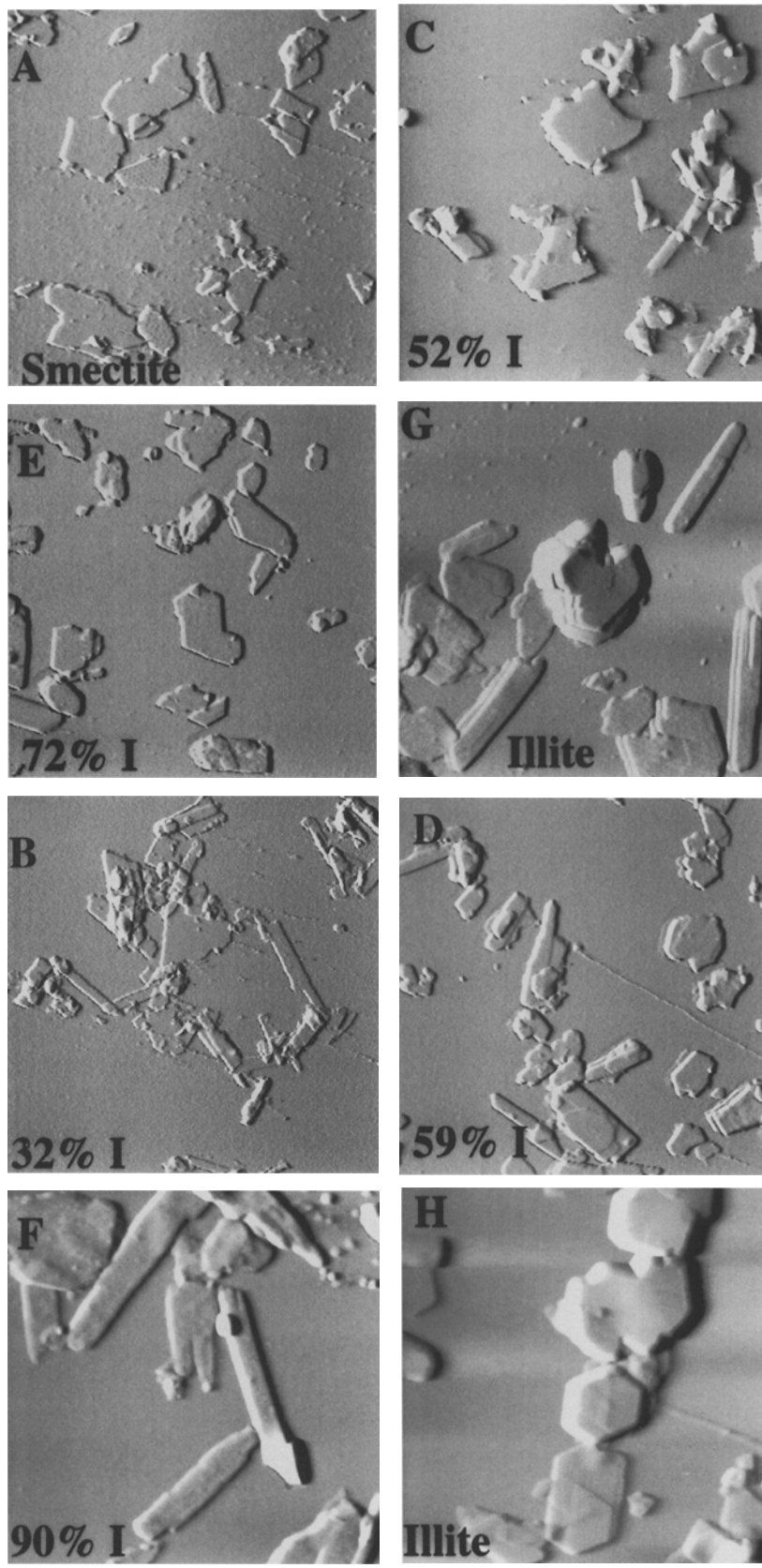

https://doi.org/10.1346/CCMN.2000.0480603 Published online by Cambridge University Press

persive spectrometers. Elemental standards included: olivine for Mg, Fe, and Mn; Amelia albite for Na, Si, and Al; microcline for K; anorthite for Ca; rutile for Ti; strontium anorthite for Sr; and chlorapatite for Cl. At least three analyses were obtained from each pellet using a 50-μm beam diameter and operating conditions of 15 kV and 25 nA. Corrections were made to the SrO concentration for interferences of the Sr L_α spectral lines by the Si K_β spectral lines (Smith and Ribbe, 1966). Approximately 1.0–2.0 g of each of the 12 unexchanged samples were analyzed using XRF at X-ray Assay Laboratories, Don Mills, Ontario. Major-element analyses are based on fused glass disks and trace elements were obtained from pressed powders. Approximate errors for XRF analyses are believed to be ±2% of the measured amount. Chemical analyses were cast into structural formulae on the basis of 22 anion equivalents and four tetrahedral cations (Newmann and Brown, 1987). Corrections were made to SiO_2 concentration because of contaminating silica phases observed by XRD.

Atomic force microscopy

Eleven I-S samples that ranged from pure smectite to pure illite were studied by atomic force microscopy (AFM) to determine particle thickness, morphology, and basal-plane area. Samples were continuously shaken for 24 h in 1 M LiCl and then centrifuged. The supernatant was decanted, new solution was added, and this process was repeated four times. Samples were then dialyzed to remove any excess LiCl and stored as suspended solutions in deionized water. I-S crystallites were dispersed onto a freshly cleaved muscovite substrate (Blum, 1994), and analyzed with a Topometrix Explorer AFM equipped with a tube scanner. Error estimates involving X and Y translations in a Cartesian coordinate system are 0.2 nm, and Z (height) is estimated at 0.2 nm. Images were "flattened" using Topometrix software which normalizes the muscovite surface to a uniform height to provide accurate height information (Blum, 1994). We measured particle thickness from flat-topped particles using the Topometrix software. In addition, we used NIH IMAGE software (version 1.59) to determine basal-plane area of both laths and plates. NIH IMAGE fits the largest ellipse into a specified area and records the perpendicular major and minor axes of that ellipse. Aspect ratio was defined as the major axis divided by the minor axis (length/width). Some operator bias may exist on the measurements because particles were selected based on particles sharpness. Particle morphologies were separated into two classifications: euhedral laths characterized by rod-like shapes with straight edges that may terminate in 60° or 120° angles, and plates characterized by equidimensional shapes that may have irregular edges and terminations (*i.e.*, anhedral plates) or straight edges terminating in 60° or 120° angles (*i.e.*, euhedral plates). The mean area and mean aspect ratio were calculated from all particles in a sample, as well as from only laths or plates.

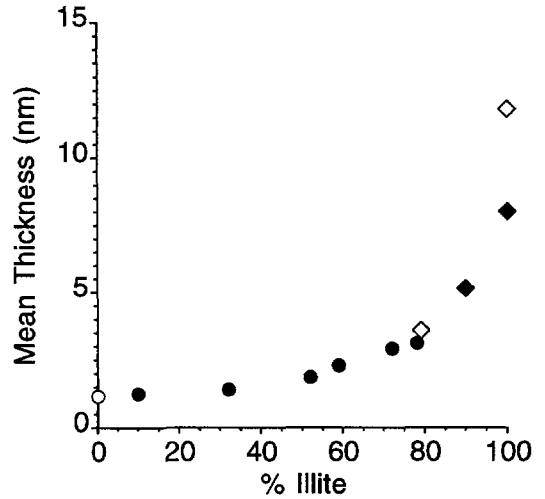

Figure 10. Mean particle thickness *vs.* % I in I-S. See Figure 7 for symbol definitions.

RESULTS

X-ray diffraction

Oriented clay-aggregate analyses. Clay minerals observed on Ponza and Gavi range from pure smectite, through a series of interstratified I-S minerals, to pure illite (Figures 2 and 3). Reichweite ordering ranges from R = 0–0.5 for smectitic I-S, through R = 1–2 for illitic I-S, to R = 3 for highly illitic I-S. Each of the alteration zones shows I-S with different layer compositions and ordering. Smectite occurs in the argillic zone; (R = 0–2) I-S with 10–82% I occurs in the propylitic zone; (R=3) I-S with 90–100% I occurs in the silicic zone; and (R = 1–3) I-S with 66–100% I occurs in the sericitic zone. We define the term illite interlayer to represent an illite layer within a MacEwan crystallite (see Altaner and Ylagan, 1997; Reynolds, 1980). Table 1 lists I-S junction probability values where $P_{I\text{-}I}$ represents the probability of an illite interlayer occurring after a given illite interlayer, and $P_{III\text{-}I}$ represents the probability of an illite layer occurring after a given sequence of three illite interlayers. Reichweite ordering in I-S from Ponza abruptly begins

←

Figure 9. AFM images of Li-saturated I-S from Ponza and Gavi. Horizontal field of view in all images is 2500 nm. (A) 93-6-8C, (B) 94-6-11C, (C) 93-6-8Q, (D) 93-6-9Q, (E) 93-6-9C, (F) 93-6-8N, (G) 93-6-10A, and (H) 93-6-10A.

https://doi.org/10.1346/CCMN.2000.0480603 Published online by Cambridge University Press

Table 2. WILDFIRE parameters used to model XRD polytype patterns of randomly oriented I-S from Ponza. Errors represent the range of best-fit patterns determined by trial and error. Orf = orientation factor where a value of 1 indicates random orientation and values <1 = preferred orientation, N_3 = number of unit cells along Z, and Hi N = maximum number of unit cells along Z.

Sample	% I	R	P_0	±	P_{cv}	±	P_{60}	±	Orf	±	N_3	Hi N	K[1]	Fe[1]
93-6-8C	0	0	0.75	0.25	0.85	0.15	0	0.1	0.85	0.03	3	12	0.01	0.16
93-6-10C	10	0	0.75	0.25	0.9	0.1	0	0.1	0.92	0.03	3	8	0.08	0.23
94-6-4C	27	0	0.8	0.2	0.75	0.08	0	0.1	0.92	0.03	3	10	0.15	0.21
93-6-8M	27	0	0.75	0.25	0.75	0.08	0	0.1	0.85	0.03	3	14	0.15	0.21
94-6-11C	32	0	0.9	0.1	0.55	0.1	0	0.1	0.85	0.05	4	14	0.16	0.18
93-6-8Q	52	0.5	0.8	0.2	0.7	0.05	0	0.1	0.8	0.05	4	10	0.3	0.2
93-6-9Q	59	1	0.9	0.1	0.6	0.05	0	0.1	0.83	0.05	4	11	0.33	0.26
93-6-9C	72	1.36	0.65	0.05	0.3	0.05	0.5	0.1	0.8	0.05	4	12	0.48	0.25
94-6-16Q	78	1.9	0.8	0.05	0.45	0.05	0.4	0.1	0.85	0.05	6	18	0.51	0.26
93-6-8N	90	3	0.95	0.05	0.33	0.05	0	0.1	0.9	0.05	7	21	0.62	0.15
93-6-10G	96	3	0.95	0.05	0.3	0.05	0	0.1	0.93	0.05	8	24	0.63	0.09
93-6-8W	100	3	1	0.05	0	0.05	0	0.1	1	0.05	7	21	0.75	0.2
93-6-9J	66	1	0.9	0.1	0.4	0.05	0	0.1	0.98	0.05	4	12	0.42	0.03
94-6-16C	67	1.13	0.88	0.05	0.35	0.05	0	0.1	0.85	0.05	5	15	0.45	0.05
93-6-9L I	79	1.5	0.85	0.05	0.75	0.05	0	0.1	0.85	0.05	6	16	0.588	0.01
94-6-16F[2]	91	3	0.85	0.05	0.8	0.05	0	0.1	0.9	0.05	7	21	0.65	0.02
94-6-16T	93	3	0.95	0.05	0.25	0.05	0	0.1	0.95	0.05	8	24	0.74	0.05
94-6-16R	96	3	0.95	0.05	0.3	0.05	0	0.1	0.93	0.05	8	24	0.71	0.06
93-6-9M[3]	98	3	1	0.05	0.1	0.05	0	0.1	0.95	0.05	8	40	0.75	0.05
93-6-10A[4]	100	3	1	0.05	0.1	0.05	0	0.1	0.95	0.05	8	40	0.75	0.05

[1] Based on EMP of Sr-saturated samples (see Table 4).
[2] Best-fit included 30% discrete *tv*-1*M* illite with parameters of P_0 = 0.85, P_{CV} = 0.05, P_{60} = 0, N_3 = 8, K = 0.75, and Fe = 0.03.
[3] Best-fit included 8% discrete $2M_1$ with parameters of N_3 = 9, K = 0.75, Fe = 0.05.
[4] Best-fit included 15% discrete $2M_1$ with parameters of N_3 = 9, K = 0.75, Fe = 0.05.

to develop at $P_1 \sim 0.45$ (Figure 4). Similar variations in I-S ordering have been observed for other hydrothermal samples from Japan and Colorado (Inoue *et al.*, 1990; Bethke *et al.*, 1986). Interestingly, partial short-range ordering ($0 < R < 1$) seems to best model I-S containing 45–60% I.

Structural analyses. XRD patterns of randomly oriented I-S from alteration zones at Ponza indicate three-dimensional layer stacking and octahedral cation ordering changes during illitization (Figure 5). Calculated XRD patterns successfully simulate the peak positions, intensities, and breadths using parameters that control the proportion of *cv* sites (P_{cv}) and rotational disorder for a range of I-S minerals (Figure 6). Reynolds (1992) characterized rotational disorder by two parameters: (1) P_0, defined as the fraction of 0° rotations between adjacent illite interlayers *versus* *n*120° rotations, where n = 1 or 2, and (2) P_{60}, defined as the fraction of non-zero degree rotations that are of the type *n*60° (where n = 1, 3, or 5). As illitization proceeds, I-S samples from Ponza systematically change from *cv* to *tv* and *n*120° rotational disorder decreases, *i.e.*, P_0 increases (Figure 7). These results indicate that I-S from Ponza progressively changes from turbostratic, *cv*-smectite to 1*M*, *tv*-illite. In addition, the two most illitic samples from the sericitic zone also contain authigenic $2M_1$ illite (5–15%). Similar changes in the octahedral vacancy position have been documented in hydrothermal I-S from Slovakia (Drits *et al.*, 1996); however, unlike McCarty and Reynolds (1995), no observable trends are found in the amount of 60° rotational disorder. Table 2 lists the parameters used to model I-S polytypes and cation ordering from Ponza. Most samples follow the *cv* to *tv* transition as illitization proceeds except for two I-S samples from the sericitic zone (93-6-9L and 94-6-16F, see Table 2, Figure 6F). Why these two samples do not follow a similar trend is unclear.

Errors in P_{cv} do not change greatly as a function of illitization; however, errors in P_0 and P_{60} are large for smectitic I-S and decrease with illitization (Table 2; Figure 7). In highly smectitic I-S, modeling rotational disorder (P_0 and P_{60}) is very difficult and errors are large because 2:1 layers are separated mainly by turbostratic interfaces and do not exhibit any *hkl* reflections (Reynolds, 1992). The abundance of *cv* and *tv*

→

Figure 11. Particle-thickness histograms for I-S from Ponza and Gavi. (A) 93-6-8C, (B) 94-6-11C, (C) 93-6-8Q, (D) 93-6-9Q, (E) 93-6-9C, (F) 93-6-9L1, (G) 93-6-8N, (H) 93-6-10A.

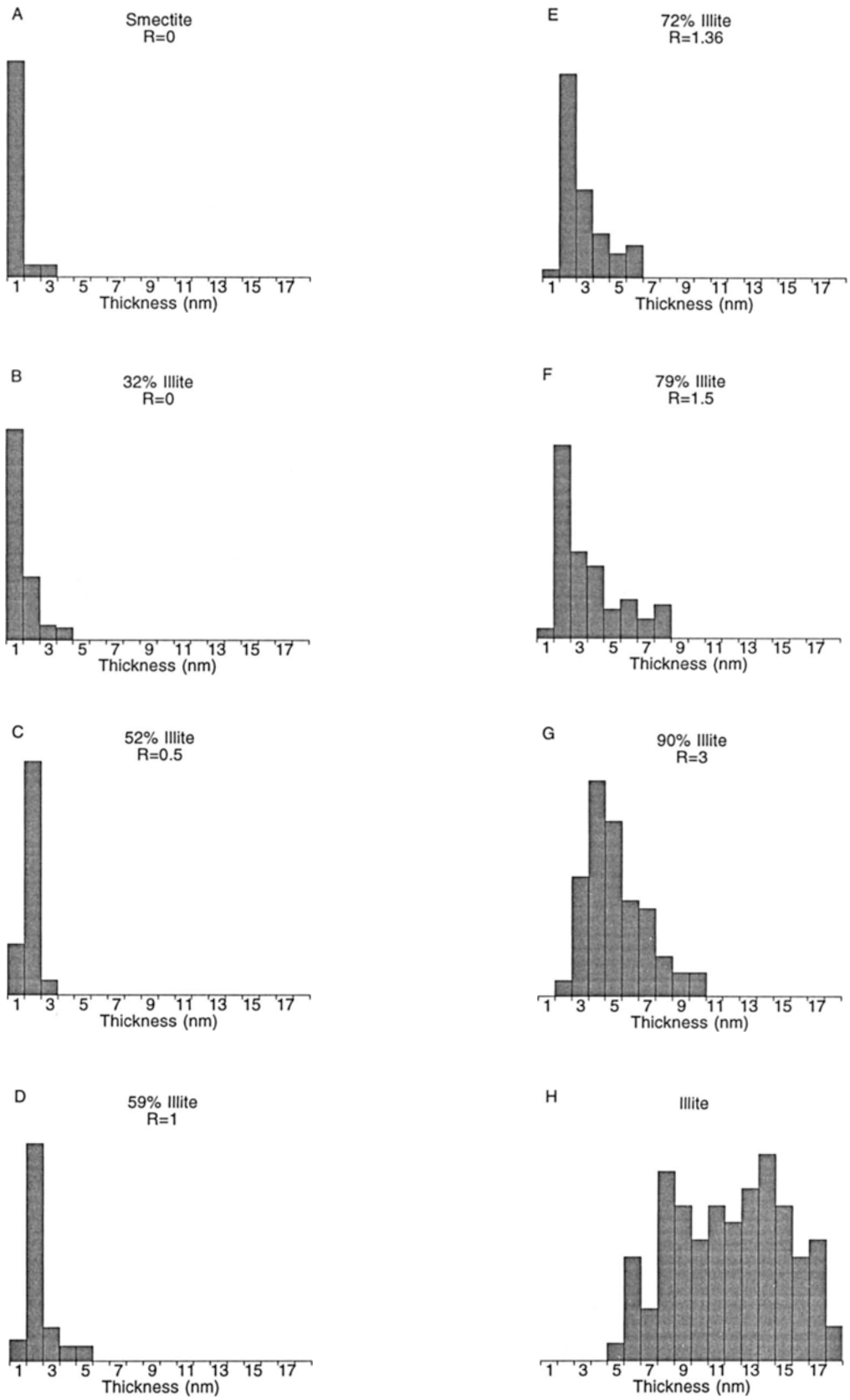

https://doi.org/10.1346/CCMN.2000.0480603 Published online by Cambridge University Press

Table 3. EMP and XRF values for major oxides in I-S from Ponza. Oxides have been cast into structural formulae.

Sample	% I	SiO_2	Al_2O_3	TiO_2	Fe_2O_3	MgO	MnO	CaO	Na_2O	K_2O	LOI
93-6-8F EMP	0	[1]56.33	17.61	0.25	3.13	4.42	0.11	2.12	0.14	0.23	—
93-6-8F XRF	0	[1]58.05	17.74	0.19	3.31	4.25	0.07	2.14	0.07	0.18	10.11
94-6-11C EMP	32	[2]53.95	24.55	0.23	3.81	3.24	0.03	0.38	0.52	2.23	—
94-6-11C XRF	32	[2]54.80	25.12	0.23	3.84	3.46	0.04	0.41	0.52	2.34	8.10
93-6-8Q EMP	52	[2]54.07	22.85	0.18	3.45	3.92	0.06	0.49	0.24	3.67	—
93-6-8Q XRF	52	[2]51.35	21.60	0.21	3.28	3.64	0.05	0.45	0.27	3.62	14.30
93-6-9Q EMP	59	[2]52.05	23.35	0.23	4.97	3.11	0.03	0.43	0.21	4.14	—
93-6-9Q XRF	59	[2]50.86	22.30	0.27	4.76	3.01	0.05	0.52	0.22	3.87	13.10
93-6-9C EMP	73	49.75	26.20	0.38	4.74	1.62	0.04	0.36	0.13	5.17	—
93-6-9C XRF	73	48.70	25.00	0.40	4.52	1.61	0.05	0.38	0.17	4.86	12.50
93-6-9L I EMP	79	50.30	30.02	0.11	0.13	1.55	0.03	0.13	0.24	6.67	—
93-6-9L I XRF	79	49.30	30.40	0.16	0.55	1.62	0.04	0.19	0.16	6.53	10.98
93-6-8N EMP	90	49.40	26.99	0.20	2.91	1.66	0.05	0.05	0.11	7.09	—
93-6-8N XRF	90	50.57	27.60	0.24	2.95	1.78	0.05	0.10	0.13	6.43	8.20
94-6-16F EMP	91	50.47	27.99	0.09	0.54	2.52	0.05	0.06	0.13	7.36	—
94-6-16F XRF	91	53.20	28.90	0.14	0.71	2.67	0.04	0.15	0.17	7.32	7.20
94-6-16T EMP	93	51.29	26.84	0.19	1.04	2.75	0.06	0.06	0.07	8.53	—
94-6-16T XRF	93	51.10	27.40	0.23	1.10	2.81	0.05	0.11	0.13	7.97	8.86
94-6-16R EMP	96	49.91	28.07	0.21	1.07	2.16	0.06	0.01	0.06	8.01	—
94-6-16R XRF	96	51.40	29.10	0.26	1.19	2.28	0.05	0.09	0.13	7.56	7.51
93-6-10G EMP	96	[2]50.52	26.70	0.24	2.08	1.69	0.07	0.05	0.25	6.91	—
93-6-10G XRF	96	[2]51.16	27.20	0.27	2.00	1.79	0.06	0.11	0.23	6.78	7.89
94-6-16D EMP	100	51.62	27.09	0.30	0.76	2.63	0.05	0.05	0.05	8.49	—
94-6-16D XRF	100	52.80	28.20	0.33	0.82	2.78	0.05	0.10	0.10	8.07	6.46

[1] Indicates analysis corrected for 5 wt. % silica impurity.
[2] Indicates analysis corrected for 2 wt. % silica impurity.

Table 4. EMP values for major oxides in Sr-saturated I-S from Ponza. Oxides have been cast into structural formulae.

Sample	% I	SiO_2	Al_2O_3	TiO_2	Fe_2O_3	MgO	MnO	CaO	Na_2O	K_2O	SrO	SUM
93-6-8C	0	[1]53.36	16.82	0.29	3.11	3.47	0.00	0.27	0.04	0.13	3.44	80.93
93-6-10C	10	49.92	21.64	0.15	4.16	1.76	0.00	0.26	0.12	0.87	3.37	82.25
94-6-11A	15	[1]51.48	19.80	0.24	2.54	2.20	0.00	0.30	0.08	0.64	3.01	80.28
94-6-3M	20	[2]50.05	21.32	0.34	3.50	1.92	0.00	0.28	0.35	1.79	3.55	83.11
93-6-3M	27	[2]49.96	21.74	0.19	3.82	2.00	0.00	0.21	0.06	1.57	3.48	83.05
94-6-4C	27	[2]48.61	19.98	0.17	3.58	2.06	0.00	0.32	0.07	1.54	2.87	79.18
94-6-11C	32	[2]50.61	23.35	0.19	3.39	2.05	0.00	0.21	0.10	1.79	3.17	84.85
94-6-3T	45	[2]48.46	21.79	0.26	3.78	1.65	0.00	0.19	0.06	2.54	2.60	81.33
93-6-8Q	52	[2]45.24	20.33	0.25	3.31	2.61	0.00	0.19	0.06	2.88	2.45	77.33
94-6-4L	54	51.58	21.56	0.35	4.07	2.13	0.00	0.26	0.05	3.58	2.56	86.14
94-6-2A	57	[2]52.10	22.12	0.26	3.62	2.57	0.00	0.22	0.08	3.78	2.10	86.85
94-6-4A	58	50.21	20.84	0.28	3.78	2.13	0.00	0.18	0.05	3.53	2.19	83.18
93-6-9Q	59	[2]47.80	21.15	0.31	4.57	2.20	0.00	0.24	0.12	3.46	2.23	82.09
[3]93-6-9J	66	[2]48.40	25.53	0.10	0.51	0.95	0.00	0.23	0.29	4.47	1.29	81.76
94-6-5D	66	51.09	21.80	0.45	4.77	1.70	0.00	0.19	0.11	3.83	1.76	85.69
93-6-9D	73	48.91	24.75	0.38	3.79	1.19	0.00	0.23	0.15	4.52	1.35	85.26
94-6-16Q	78	49.91	20.76	0.27	4.70	1.70	0.00	0.23	0.28	4.99	1.24	84.07
[3]93-6-9L 1	79	48.36	29.43	0.11	0.15	1.15	0.00	0.16	0.16	6.17	0.84	86.53
94-6-16J	82	49.47	23.73	0.37	4.60	1.12	0.00	0.34	0.66	4.81	1.00	86.10
93-6-8N	90	50.83	26.25	0.20	2.89	1.28	0.00	0.15	0.15	6.56	0.83	89.14
94-6-16F	91	49.64	26.50	0.13	0.67	1.95	0.00	0.14	0.15	6.36	0.48	86.01
94-6-16R	96	50.24	27.59	0.26	1.12	1.93	0.00	0.13	0.18	7.40	0.15	89.02
[3]93-6-9M	98	47.07	31.54	0.15	0.37	0.74	0.00	0.05	0.21	8.00	0.15	88.29
93-6-10A	100	52.08	27.72	0.38	0.85	2.25	0.00	0.09	0.11	8.49	0.10	92.06

[1] Indicates analysis adjusted for 5 wt. % silica mineral impurity.
[2] Indicates analysis adjusted for 2 wt. % silica mineral impurity.
[3] Identifies altered rhyolitic intrusion from Punta d'Incenso.

https://doi.org/10.1346/CCMN.2000.0480603 Published online by Cambridge University Press

Table 3. Extended.

SUM	Structural Formula, per $O_{10}(OH)_2$
84.33	$K_{0.02}Ca_{0.16}Na_{0.02}Si_{3.95}{}^{IV}Al_{0.05}{}^{VI}Al_{1.40}Fe_{0.17}Mg_{0.46}Ti_{0.01}$
96.11	$K_{0.02}Ca_{0.16}Na_{0.00}Si_{3.98}{}^{IV}Al_{0.02}{}^{VI}Al_{1.42}Fe_{0.17}Mg_{0.43}Ti_{0.00}$
88.96	$K_{0.19}Ca_{0.03}Na_{0.07}Si_{3.64}{}^{IV}Al_{0.36}{}^{VI}Al_{1.59}Fe_{0.19}Mg_{0.33}Ti_{0.01}$
98.86	$K_{0.20}Ca_{0.03}Na_{0.07}Si_{3.62}{}^{IV}Al_{0.38}{}^{VI}Al_{1.58}Fe_{0.19}Mg_{0.34}Ti_{0.01}$
88.92	$K_{0.32}Ca_{0.04}Na_{0.03}Si_{3.68}{}^{IV}Al_{0.32}{}^{VI}Al_{1.51}Fe_{0.18}Mg_{0.40}Ti_{0.00}$
98.77	$K_{0.33}Ca_{0.03}Na_{0.04}Si_{3.68}{}^{IV}Al_{0.32}{}^{VI}Al_{1.51}Fe_{0.18}Mg_{0.39}Ti_{0.01}$
88.51	$K_{0.36}Ca_{0.03}Na_{0.03}Si_{3.59}{}^{IV}Al_{0.41}{}^{VI}Al_{1.49}Fe_{0.26}Mg_{0.32}Ti_{0.01}$
98.96	$K_{0.35}Ca_{0.04}Na_{0.03}Si_{3.62}{}^{IV}Al_{0.38}{}^{VI}Al_{1.49}Fe_{0.25}Mg_{0.32}Ti_{0.01}$
88.39	$K_{0.46}Ca_{0.03}Na_{0.02}Si_{3.46}{}^{IV}Al_{0.54}{}^{VI}Al_{1.61}Fe_{0.25}Mg_{0.17}Ti_{0.02}$
98.19	$K_{0.44}Ca_{0.03}Na_{0.02}Si_{3.49}{}^{IV}Al_{0.51}{}^{VI}Al_{1.60}Fe_{0.24}Mg_{0.17}Ti_{0.02}$
89.18	$K_{0.58}Ca_{0.00}Na_{0.03}Si_{3.44}{}^{IV}Al_{0.56}{}^{VI}Al_{1.86}Fe_{0.00}Mg_{0.16}Ti_{0.00}$
99.93	$K_{0.57}Ca_{0.01}Na_{0.02}Si_{3.39}{}^{IV}Al_{0.61}{}^{VI}Al_{1.85}Fe_{0.03}Mg_{0.17}Ti_{0.00}$
88.46	$K_{0.63}Ca_{0.00}Na_{0.01}Si_{3.45}{}^{IV}Al_{0.55}{}^{VI}Al_{1.68}Fe_{0.15}Mg_{0.17}Ti_{0.01}$
98.04	$K_{0.56}Ca_{0.00}Na_{0.02}Si_{3.46}{}^{IV}Al_{0.54}{}^{VI}Al_{1.69}Fe_{0.15}Mg_{0.18}Ti_{0.01}$
89.23	$K_{0.65}Ca_{0.00}Na_{0.02}Si_{3.47}{}^{IV}Al_{0.53}{}^{VI}Al_{1.74}Fe_{0.03}Mg_{0.26}Ti_{0.00}$
100.50	$K_{0.61}Ca_{0.00}Na_{0.02}Si_{3.49}{}^{IV}Al_{0.51}{}^{VI}Al_{1.73}Fe_{0.04}Mg_{0.26}Ti_{0.00}$
90.82	$K_{0.74}Ca_{0.00}Na_{0.00}Si_{3.50}{}^{IV}Al_{0.50}{}^{VI}Al_{1.66}Fe_{0.05}Mg_{0.28}Ti_{0.00}$
99.76	$K_{0.69}Ca_{0.00}Na_{0.02}Si_{3.47}{}^{IV}Al_{0.53}{}^{VI}Al_{1.67}Fe_{0.06}Mg_{0.28}Ti_{0.01}$
89.56	$K_{0.71}Ca_{0.00}Na_{0.00}Si_{3.44}{}^{IV}Al_{0.56}{}^{VI}Al_{1.73}Fe_{0.06}Mg_{0.22}Ti_{0.01}$
99.57	$K_{0.65}Ca_{0.00}Na_{0.02}Si_{3.44}{}^{IV}Al_{0.56}{}^{VI}Al_{1.73}Fe_{0.06}Mg_{0.23}Ti_{0.01}$
88.51	$K_{0.61}Ca_{0.00}Na_{0.03}Si_{3.51}{}^{IV}Al_{0.49}{}^{VI}Al_{1.70}Fe_{0.11}Mg_{0.18}Ti_{0.01}$
97.49	$K_{0.59}Ca_{0.00}Na_{0.03}Si_{3.51}{}^{IV}Al_{0.49}{}^{VI}Al_{1.71}Fe_{0.10}Mg_{0.18}Ti_{0.01}$
91.05	$K_{0.74}Ca_{0.00}Na_{0.00}Si_{3.51}{}^{IV}Al_{0.49}{}^{VI}Al_{1.68}Fe_{0.04}Mg_{0.27}Ti_{0.02}$
99.71	$K_{0.68}Ca_{0.00}Na_{0.01}Si_{3.49}{}^{IV}Al_{0.51}{}^{VI}Al_{1.69}Fe_{0.04}Mg_{0.27}Ti_{0.02}$

Table 4. Extended.

Structural Formula, per $O_{10}(OH)_2$
$K_{0.01}Sr_{0.15}Ca_{0.02}Na_{0.00}Si_{3.97}{}^{IV}Al_{0.03}{}^{VI}Al_{1.44}Fe_{0.17}Mg_{0.38}Ti_{0.02}$
$K_{0.08}Sr_{0.14}Ca_{0.02}Na_{0.00}Si_{3.70}{}^{IV}Al_{0.30}{}^{VI}Al_{1.59}Fe_{0.23}Mg_{0.19}Ti_{0.00}$
$K_{0.06}Sr_{0.13}Ca_{0.02}Na_{0.01}Si_{3.85}{}^{IV}Al_{0.15}{}^{VI}Al_{1.60}Fe_{0.714}Mg_{024}{}^{Ti}{}_{0.01}$
$K_{0.17}Sr_{0.15}Ca_{0.02}Na_{0.05}Si_{3.70}{}^{IV}Al_{0.30}{}^{VI}Al_{1.55}Fe_{0.19}Mg_{0.21}Ti_{0.02}$
$K_{0.15}Sr_{0.15}Ca_{0.02}Na_{0.00}Si_{3.68}{}^{IV}Al_{0.32}{}^{VI}Al_{1.57}Fe_{0.21}Mg_{0.22}Ti_{0.01}$
$K_{0.15}Sr_{0.13}Ca_{0.03}Na_{0.01}Si_{3.74}{}^{IV}Al_{0.26}{}^{VI}Al_{1.55}Fe_{0.21}Mg_{0.24}Ti_{0.00}$
$K_{0.16}Sr_{0.13}Ca_{0.02}Na_{0.01}Si_{3.64}{}^{IV}Al_{0.36}{}^{VI}Al_{1.62}Fe_{0.18}Mg_{0.22}Ti_{0.01}$
$K_{0.24}Sr_{0.11}Ca_{0.02}Na_{0.00}Si_{3.65}{}^{IV}Al_{0.35}{}^{VI}Al_{1.59}Fe_{0.21}Mg_{0.19}Ti_{0.01}$
$K_{0.29}Sr_{0.11}Ca_{0.02}Na_{0.00}Si_{3.61}{}^{IV}Al_{0.39}{}^{VI}Al_{1.52}Fe_{0.20}Mg_{0.31}Ti_{0.02}$
$K_{0.33}Sr_{0.11}Ca_{0.02}Na_{0.00}Si_{3.69}{}^{IV}Al_{0.31}{}^{VI}Al_{1.51}Fe_{0.22}Mg_{0.23}Ti_{0.02}$
$K_{0.34}Sr_{0.09}Ca_{0.02}Na_{0.01}Si_{3.68}{}^{IV}Al_{0.32}{}^{VI}Al_{1.53}Fe_{0.19}Mg_{0.27}Ti_{0.01}$
$K_{0.33}Sr_{0.09}Ca_{0.01}Na_{0.00}Si_{3.71}{}^{IV}Al_{0.29}{}^{VI}Al_{1.52}Fe_{0.21}Mg_{0.23}Ti_{0.02}$
$K_{0.33}Sr_{0.10}Ca_{0.02}Na_{0.02}Si_{3.61}{}^{IV}Al_{0.39}{}^{VI}Al_{1.49}Fe_{0.26}Mg_{0.25}Ti_{0.02}$
$K_{0.42}Sr_{0.06}Ca_{0.02}Na_{0.04}Si_{3.59}{}^{IV}Al_{0.41}{}^{VI}Al_{1.83}Fe_{0.03}Mg_{0.10}Ti_{0.00}$
$K_{0.35}Sr_{0.07}Ca_{0.01}Na_{0.02}Si_{3.67}{}^{IV}Al_{0.33}{}^{VI}Al_{1.52}Fe_{0.26}Mg_{0.18}Ti_{0.02}$
$K_{0.42}Sr_{0.06}Ca_{0.02}Na_{0.02}Si_{3.53}{}^{IV}Al_{0.47}{}^{VI}Al_{1.64}Fe_{0.21}Mg_{0.13}Ti_{0.02}$
$K_{0.47}Sr_{0.05}Ca_{0.02}Na_{0.04}Si_{3.68}{}^{IV}Al_{0.32}{}^{VI}Al_{1.48}Fe_{0.26}Mg_{0.19}Ti_{0.01}$
$K_{0.56}Sr_{0.03}Ca_{0.01}Na_{0.02}Si_{3.42}{}^{IV}Al_{0.58}{}^{VI}Al_{1.87}Fe_{0.00}Mg_{0.12}Ti_{0.00}$
$K_{0.44}Sr_{0.04}Ca_{0.03}Na_{0.09}Si_{3.56}{}^{IV}Al_{0.44}{}^{VI}Al_{1.57}Fe_{0.25}Mg_{0.12}Ti_{0.02}$
$K_{0.58}Sr_{0.03}Ca_{0.01}Na_{0.02}Si_{3.53}{}^{IV}Al_{0.47}{}^{VI}Al_{1.67}Fe_{0.15}Mg_{0.13}Ti_{0.01}$
$K_{0.58}Sr_{0.02}Ca_{0.01}Na_{0.02}Si_{3.53}{}^{IV}Al_{0.47}{}^{VI}Al_{1.75}Fe_{0.04}Mg_{0.21}Ti_{0.00}$
$K_{0.65}Sr_{0.00}Ca_{0.00}Na_{0.02}Si_{3.48}{}^{IV}Al_{0.52}{}^{VI}Al_{1.73}Fe_{0.06}Mg_{0.20}Ti_{0.01}$
$K_{0.71}Sr_{0.00}Ca_{0.00}Na_{0.03}Si_{3.30}{}^{IV}Al_{0.70}{}^{VI}Al_{1.90}Fe_{0.02}Mg_{0.08}Ti_{0.00}$
$K_{0.73}Sr_{0.00}Ca_{0.00}Na_{0.01}Si_{3.50}{}^{IV}Al_{0.50}{}^{VI}Al_{1.69}Fe_{0.04}Mg_{0.23}Ti_{0.02}$

sites can be determined in highly smectitic samples because calculated patterns predict differences in the line profiles between 20–25 °2θ. There is less error in illitic I-S because *hkl* peaks are well defined due to greater ordering between 2:1 layers.

In general, calculated XRD patterns successfully modeled experimental patterns; however some minor differences exist. For example, the (11*l*) reflections in the experimental patterns have consistently higher *d* values than those in the calculated patterns. In illitic I-S with *tv* sites, the intensity ratio of the $(11\bar{1})$:$(11\bar{2})$ in the calculated patterns is always greater than in the experimental patterns (*e.g.*, Figure 6G and 6H). In addition, experimental patterns of illitic, highly *cv* samples have small peaks consistent with (021) and $(11\bar{1})$ reflections, whereas calculated patterns do not contain them (Figure 6F). The model of Drits *et al.* (1984) produced (021) and $(11\bar{1})$ peaks by ordering the vacancy of a *cv* structure into a single M2 site, whereas WILDFIRE may not produce these reflections because there is an equal probability the vacancy resides in either of the two M2 sites. Explanations for these minor differences between calculated and experimental patterns remain unclear and future refinements in the computer modeling of XRD patterns of the *cv* and *tv* forms may provide greater insight.

Comparison of XRF and EMP chemical analyses

Although elemental oxide analyses differ slightly between EMP and XRF (Table 3), EMP provides accurate chemical analysis of I-S clay minerals because structural formulae (Table 4) derived from both techniques are consistent. The difference in oxides may arise because EMP analyses are obtained from pressed pellets with rough surfaces and high porosites. In general, structural formulae based on EMP differ from XRF by at most 8%, and more often by only 2–5%. For example, the average difference between EMP and XRF structural formulae for interlayer K is 5.4%, octahedral Mg is 2.4%, octahedral Al is 0.5%, and tetrahedral Si is 0.6%.

Chemical variations during illitization

Sr-saturated I-S samples from Ponza show systematic chemical changes associated with smectite illitization: exchangeable cations decrease, fixed K increases, and tetrahedral Al for Si substitution increases (Figure 8A–8C). Table 4 lists the EMP oxide values and structural formulae for Sr-saturated I-S from Ponza. The increase in layer charge from −0.36 in smectite to −0.76 in the most illitic sample can be attributed to increasing tetrahedral charge because octahedral charge shows no systematic variation (Figure 8D–8F). Smectite from the argillic zone can be considered montmorillonite because most of the layer charge is developed in the octahedral sheet (*e.g.*, sample 93-6-8C, Table 4). However, smectitic I-S with as

Table 5. Abundance of different particle shapes and mean particle measurements based on AFM. (±) = 95% confidence interval.

Sample	%I	N[1]	% Laths	% Plates	Area ($\times 10^3$ mm^2)	±	Aspect ratio	±	N[2]	Thickness (nm)
93-6-8C	0	286	8	92	52.69	7.25	1.91	0.09	145	1.15
93-6-10C	10	178	16	94	41.86	5.59	2.32	0.21	109	1.26
94-6-11C	32	286	50	50	42.52	4.06	2.98	0.21	153	1.43
93-6-8Q	52	193	44	56	59.75	7.52	2.96	0.27	122	1.88
93-6-9Q	59	268	40	60	47.68	4.04	3.12	0.27	185	2.29
93-6-9D	72	210	27	73	48.92	5.05	2.37	0.20	146	2.92
94-6-16Q	78	137	36	64	69.25	7.39	2.35	0.21	93	3.11
93-6-8N	90	126	35	65	166.32	20.77	2.94	0.29	76	5.13
93-6-8W	100	140	86	14	67.12	9.86	3.86	0.31	98	8.01
93-6-9L	79	145	54	46	71.73	5.44	2.59	0.15	102	3.58
93-6-10A	100	166	46	54	185.50	22.15	2.35	0.19	128	11.8

[1] Number of particles measured to determine mean particle area and aspect ratio.
[2] Number of particles measured to determine mean crystallite thickness.

little as 10% I from the adjacent propylitic zone is beidellitic in composition because a large proportion of charge is derived from tetrahedral substitutions (*e.g.*, sample 93-6-10C, Table 4). There are few systematic variations in the composition of the octahedral sheet during illitization, except that I-S from the sericitic zone contains significantly more ^{VI}Al and less Fe compared to I-S from other alteration zones (Figure 8G–8H). Comparison of untreated I-S and Sr-exchanged I-S indicates that exchangeable cations include Ca, Na, and Mg (Tables 3 and 4). After Sr-exchange, the Mg contents of I-S decreased and octahedral occupancies decreased from anomalously high values (≤2.13) to more ideal dioctahedral values (2.00 ± 0.04) for cations (*e.g.*, samples 94-6-11C and 93-6-8Q, Tables 3 and 4).

Sericitic zone I-S samples with a hyaloclastite precursor (samples 94-6-16F, 94-6-16R, and 93-6-10A) differ chemically from sericitic zone I-S samples with a silicic intrusion precursor (93-6-9J, 93-6-9L1, and 93-6-9M). For example, sericitic zone I-S originating from the altered intrusion contains high octahedral Al (1.80–1.90 cations per half-formula unit), high tetrahedral Al (0.41–0.70 cations), and low Mg (0.08–0.12 cations), whereas sericitic zone clays originating from the hyaloclastite contain lower octahedral Al (1.69–1.75 cations), lower tetrahedral Al (0.47–0.52 cations), and higher Mg (0.21–0.23 cations).

Cis-trans changes (P_{cv}) are correlated with total layer charge, tetrahedral layer charge, and fixed K because these parameters must change systematically with illitization (Figure 7A). Correlations are difficult to determine for P_0 because of greater uncertainties (Figure 7B). Octahedral sheet chemistries show no systematic changes with illitization and therefore cannot be correlated with P_{cv} or P_0.

Morphological analysis

AFM analyses indicate that particle morphologies evolve in three different ways during illitization: (1) particle shape changes from anhedral plates to laths, and then to euhedral plates, (2) particle thickness increases, and (3) particle area remains constant until particles become highly illitic and area increases. Table 5 summarizes the particle measurements of I-S from Ponza. Smectitic I-S (≤10% I) contains predominantly anhedral plates with some laths (Figure 9A), I-S with 30–50% I (R = 0) contains laths and anhedral plates in equal proportions (Figure 9B and 9C), and illitic I-S with 60–100% I (R = 1–3) contains laths and euhedral plates in roughly equal proportions (Figure 9D–9G). Hexagons occur in the most illitic samples (Figure 9H).

The mean particle aspect ratio (length/width) reflects the morphological progression of anhedral plates to laths, and then to euhedral plates during illitization (Table 5). For example, the mean particle aspect ratio is ~2 for pure smectite, ~3 for I-S with 30–60% I, and then decreases to ~2.5 for I-S with >60% I. The aspect ratio of laths follows a similar trend, but the aspect ratio of plates progressively decreases with illitization. One illite sample from the silicic zone (93-6-8W) differs from the trend described above. Unlike the other highly illitic samples that contain ~50% laths, 93-6-8W is composed of 85–90% laths and therefore has a greater aspect ratio of ~4 (Table 5).

As illitization proceeds, mean particle thickness increases, particularly for the most illitic samples (Figure 10). Particle-thickness histograms indicate that smectitic I-S is composed primarily of 1-nm thick particles (Figure 11A and 11B), and I-S with 50–80% I contains particles that average 2–4 nm (Figure 11C–11F). In highly illitic I-S, mean thickness ranges from 5 to 12 nm (Figure 11G and 11H).

Mean particle area does not change from pure smectite to I-S with 80% I; however particle area progressively increases from 90 to 100% illite (Figure 12A). Most of the highly illitic I-S samples (90–100% I) have much larger particle areas than less illitic I-S. Sample 93-6-8W does not follow this trend because it

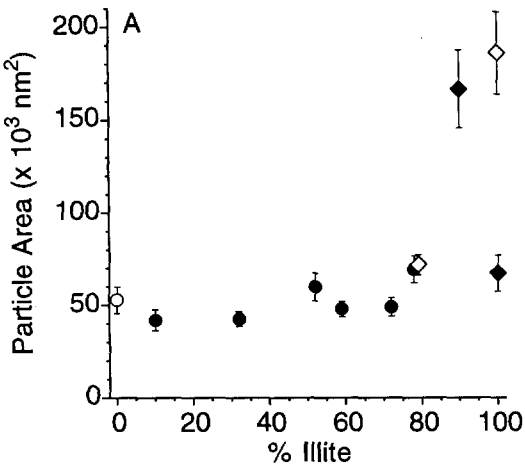

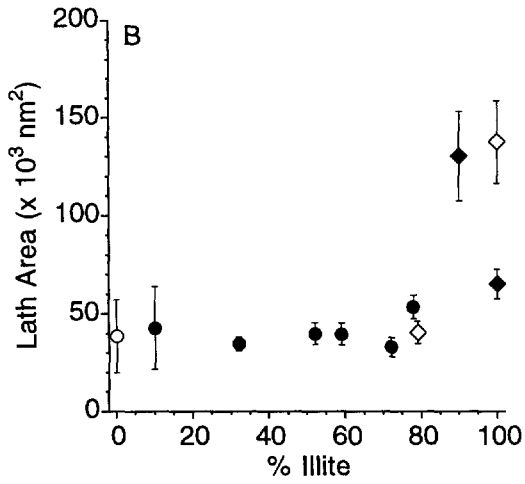

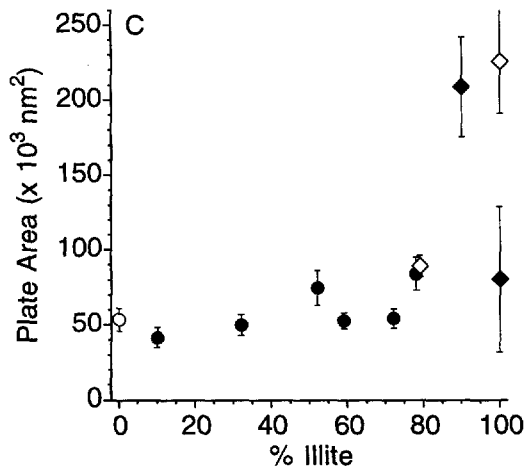

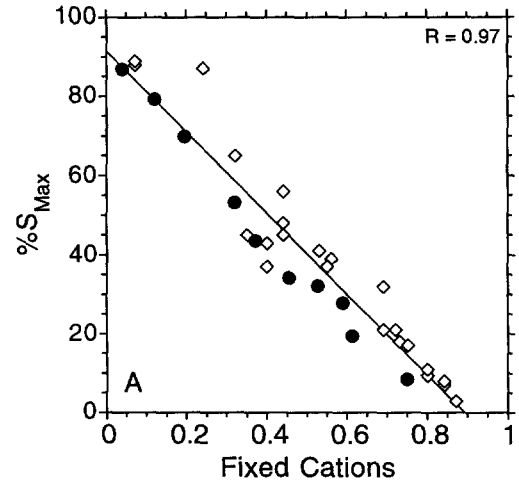

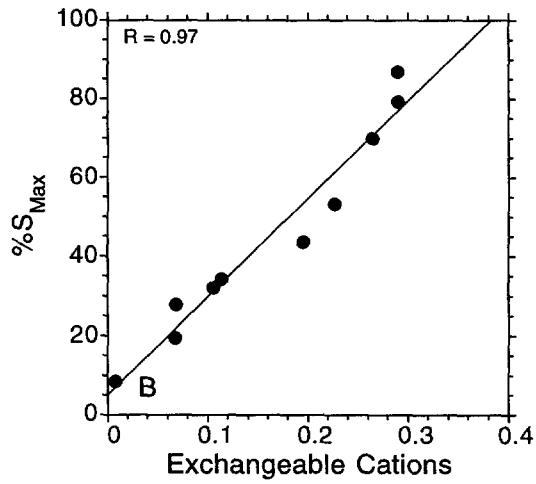

Figure 13. (A) % S_{max} (maximum value of smectite in I-S based on average particle thickness) *vs.* fixed cations, with $\%S_{max} = 91.33 - 102.35 \times FIX$. (B) % S_{max} *vs.* exchangeable cations, with $\% S_{max} = 5.16 + 247.94 \times EXCH$. (◇) = TEM and HRTEM data of Środoń *et al.* (1992), (●) = AFM data this study.

is composed of 85–90% laths which tend to have smaller areas than the plates (Figure 12B and 12C). Similarly, separate measurements of either lath or plate area do not show any significant changes until 90% I, where both lath and plate areas increase.

←

Figure 12. Particle area *vs.* % I in I-S from Ponza and Gavi. (A) all particles, (B) lath-like particles, (C) plate-like particles. Error bars represent 95% confidence intervals. See Figure 7 for symbol definitions.

https://doi.org/10.1346/CCMN.2000.0480603 Published online by Cambridge University Press

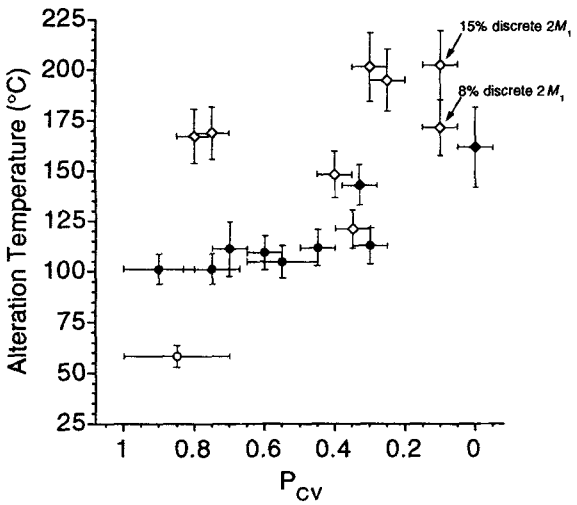

Figure 14. Alteration temperature *vs.* proportion of *cis*-vacant sites in I-S. Alteration temperatures are derived from stable-isotopic and fluid-inclusion data from Ylagan (1996).

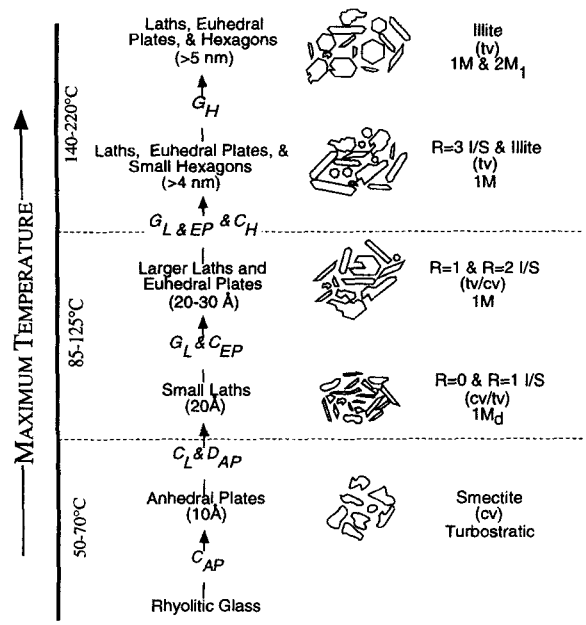

Figure 15. Schematic reaction mechanisms of smectite illitization on Ponza in terms of alteration temperature, R ordering, polytype, and particle shape. C_{AP} = crystallization of anhedral plates, D_{AP} = dissolution of anhedral plates, C_L = crystallization of laths, G_L = crystal growth of laths, C_{EP} = crystallization of euhedral plates, G_{EP} = growth of euhedral plates, C_H = crystallization of hexagons, G_H = crystal growth of hexagons.

DISCUSSION

Chemical changes during illitization

The major chemical changes (increasing K and ^{IV}Al, decreasing Si and exchangeable cations) in I-S minerals from Ponza island are similar to chemical variations in I-S from other sedimentary (Brusewitz, 1986; Środoń *et al.*, 1986; Nadeau and Bain, 1986; Awwiller, 1993) and hydrothermal environments (Inoue *et al.*, 1978; Inoue and Utada, 1983; Šucha *et al.*, 1992). In contrast to other studies of illitization in bentonite (Brusewitz, 1986; Środoń *et al.*, 1986), shale (Lynch *et al.*, 1997; Awwiller, 1993), and hydrothermal settings (Inoue *et al.*, 1978; Inoue and Utada, 1983), octahedral Mg in I-S from Ponza is unusually high and shows no decrease with illitization. We attribute Mg-rich I-S at Ponza to hydrothermal alteration involving seawater, which is rich in Mg. Stable-isotopic and fluid-inclusion data (Ylagan, 1996) support the hydrothermal alteration at Ponza involving seawater. Experimental and natural-system studies of chemical interactions between rhyolite glass and seawater indicate that clay minerals extract significant amounts of Mg from seawater during glass alteration (Zielinski, 1982; Hajish and Chandler, 1981; Shiraki *et al.*, 1987; Christidis and Dunham, 1993). Permeability also seems to have affected the amount of Mg enrichment because I-S derived from alteration of the brecciated rhyolitic hyaloclastite contains more Mg than I-S derived from alteration of a massive rhyolitic intrusion. This difference suggests that the Mg-rich hydrothermal fluids interacted more extensively with the hyaloclastite than with the intrusion.

I-S from Ponza evolves towards a phengite composition rather than a muscovite. In the most illitic samples, layer charge is not derived exclusively from the tetrahedral sheet as in muscovite, but it is distributed between the octahedral and tetrahedral sheets similar to phengite. Numerous studies support this result because octahedral Mg remains relatively high (≥0.10 cations per half unit cell) in highly illitic samples from bentonite and hydrothermal settings (Pearce and Clayton, 1995; Inoue *et al.*, 1978; Brusewitz, 1986; Środoń *et al.*, 1986, 1992; Šucha *et al.*, 1992; Eberl *et al.*, 1987; Nadeau and Bain, 1986). Some exceptions are found in hydrothermal sericites from Colorado (Eberl *et al.*, 1987) and Japan (Środoń and Eberl, 1984).

For extrapolation to end-member components of illite and smectite, XRD underestimates the total proportion of smectite sites, particularly for illitic I-S because XRD is unable to characterize smectite sites located at the tops and bottoms of diffracting domains (Altaner *et al.*, 1988). More accurate determinations of the total proportion of smectite sites in I-S include fixed cation content and particle-thickness data (Środoń *et al.*, 1992). The parameter $\%S_{max}$ (the total proportion of smectite sites in I-S) may be calculated from Środoń *et al.* (1992). Extrapolations indicate that end-member illite from Ponza has a composition of 0.89 fixed interlayer cations and the smectite component has a composition of ~0.38 exchangeable cations

https://doi.org/10.1346/CCMN.2000.0480603 Published online by Cambridge University Press

(Figure 13A and 13B). These compositions are similar to I-S from many different localities and geologic settings (Środoń *et al.*, 1992).

Structural changes and temperatures of alteration

We interpret the progressive structural transitions in these I-S minerals from Ponza (*cv* and turbostratic smectite, to *cv/tv* and $1M_d$ I-S, to *tv* and $1M$ illite, and finally to $2M_1$ illite) to be primarily a response to increasing temperature. Although other parameters (*e.g.*, permeability, K^+ availability) may influence the transition, they do not seem to be primary controls. Evidence suggesting these parameters do not influence the transition include: (1) original hyaloclastite was of uniform composition, (2) hydrothermal alteration occurred in a submarine environment, and (3) the transition appears to be a geologically abrupt event in which fluids are derived from seawater (Ylagan, 1996). For example, estimated alteration temperatures from fluid-inclusion and oxygen-isotope analyses (Ylagan, 1996) correlate very well with the proportion of *cv* sites and to a lesser extent the degree of rotational disorder (Figure 14). A similar evolution of I-S structural forms with temperature has been observed in laboratory experiments (Warshaw, 1960; Velde, 1965; Mukhamet-Galeyev *et al.*, 1985) and hydrothermally altered volcaniclastics (Inoue *et al.*, 1987; Drits *et al.*, 1993, 1996). The most illitic samples from Ponza contain $1M$ and $2M_1$ illite and have estimated alteration temperatures between 200–225°C which is similar to the range in temperatures for the $1M$ to $2M_1$ transition from other studies of natural systems by Velde and Hower (1963) and Di Marco *et al.* (1989). Unlike the conclusions of McCarty and Reynolds (1995), *cv-tv* and rotational transitions at Ponza do not seem to correlate with octahedral Mg and Fe contents.

Mechanism of smectite illitization on Ponza

I-S from Ponza undergoes significant morphological, chemical, and structural changes with increased alteration temperature that support a DC mechanism for smectite illitization. Figure 15 illustrates a proposed mechanism for smectite illitization on Ponza which has been developed primarily from morphological observations and other mineralogical and geochemical data. Alternatively, the mechanism of I-S and illite formation may not involve illitization of smectite precursors but rather direct crystallization of I-S and illite crystallites from rhyolite glass. Laboratory experiments (Small *et al.* 1992a, 1992b) support the direct precipitation model, but because of its greater complexity, we will further describe the multi-step model. Temperatures for each alteration zone are from Ylagan (1996). In the argillic zone (T = 50–65°C), temperatures were insufficient to cause complete alteration of the hyaloclastite. Thin (1 nm thick) anhedral plates of turbostratic, *cv*-smectite crystallized.

In the propylitic zone (T = 85–125°C), the anhedral plates dissolved and small, thin (1–2 nm) laths crystallized. This step corresponds to the transition from smectite to (R = 0) I-S. Although other studies of hydrothermal I-S have proposed that illitization in this interval occurs by K^+ fixation (Inoue *et al.*, 1987), illitization to (R = 0) I-S on Ponza must involve a DC mechanism on the basis of abrupt changes in morphology, isotopic composition, and layer charge. For example, anhedral plates dominate in the pure smectite samples (Figure 9A), whereas laths are found in (R = 0) I-S (Figure 9B). The measured $\delta^{18}O_{smectite}$ is ~22.0‰ and $\delta^{18}O_{(R=0)\,I\text{-}S}$ is ~15.5‰ (Ylagan, 1996) and indicate significant isotopic exchange occurred. Pure smectite from Ponza is montmorillonite in composition, having a low layer charge of −0.35 derived from octahedral site substitutions (Table 4). In contrast, (R = 0) I-S has a higher layer charge of −0.43 to −0.57 that is largely derived from tetrahedral substitutions (Table 4).

At higher grades of alteration within the propylitic zone, I-S continues to undergo dissolution and crystallization reactions associated with the R = 0 to R = 1 transition. Anhedral plates diminish in abundance, whereas thicker (2–3 nm) laths and euhedral plates become more evident (Figure 9B and 9D). Lath areas increase slightly and euhedral plates with 60° and 120° terminations crystallize. The R = 0 to R = 1 transition in Ponza I-S occurs relatively abruptly at ~45% I (Figure 4), which is consistent with a DC mechanism. The R = 0 to R = 1 transition at Ponza contrasts with a more gradual R = 0 to R = 1 transition at 65% I as observed in shale (Bethke *et al.*, 1986) and bentonite (Inoue *et al.*, 1990), where an SST mechanism was proposed (Inoue *et al.*, 1990; Lindgreen *et al.*, 1991). The progressive changes in cation ordering (Figure 7A), layer charge (Figure 8D), and isotopic composition (Ylagan, 1996) which also occur over this interval are explained by the transformation of turbostratic, *cv*, anhedral plates to *tv*(?), $1M_d$ and $1M$ laths and plates.

In the silicic and sericitic zones (140–225°C), laths and euhedral plates undergo significant crystal growth (Figures 9E, 9F, 12A, and 12C) resulting in highly illitic I-S crystallites (≥90% I with R = 3 order). Progressive changes in layer charge, isotopic composition, and polytype also support the crystal-growth model. Although significant crystal growth occurs in this stage, it is not appropriate to classify this process as Ostwald ripening as others have proposed (Inoue *et al.*, 1988; Eberl *et al.*, 1990; Christidis *et al.*, 1995). Ostwald ripening refers to crystal growth of chemically similar particles induced by a drive to minimize surface area in a chemically closed system (Baronnet, 1982). In contrast to Ostwald ripening, I-S from Ponza undergoes significant chemical changes and alteration occured in an open chemical system.

The most illitic samples from the sericitic zone contain thick (≥4 nm) hexagon-shaped particles with small basal-plane areas. The occurrence of these plates coincides with the appearance of the $2M_1$ polytype. These results suggest that the $1M$ to $2M_1$ transition occurs by a DC mechanism (Lonker and Fitz Gerald, 1990; Lee *et al.*, 1985; Mukhamet-Galeyev *et al.*, 1985; Baxter Grubb *et al.*, 1991), although Hunziker *et al.* (1986) have proposed an SST mechanism for similar evidence. Because chemical variations of I-S are relatively small in this interval, Ostwald ripening may apply (*e.g.*, Inoue and Kitagawa, 1994).

The multi-step DC model presented here is very similar to the model of Inoue *et al.* (1987) in which they proposed a three step process of K fixation, followed by DC, and then followed by Ostwald ripening. Two differences are noted: (1) the R = 0 to R = 1 transition occurs by a DC mechanism and not by a K-fixation process based on significant morphological, chemical, isotopic, and structural transitions, and (2) based on particle area measurements, crystal growth of I-S from Ponza was less significant than that observed in I-S from Japan.

CONCLUSIONS

Chemical, morphological, and structural changes of I-S from Ponza island, Italy have been characterized to describe the reaction mechanism of smectite illitization. We conclude the following: (1) Systematic chemical changes in I-S occur during illitization and include increasing K and Al, and decreasing Si, Fe, and exchangeable cations. However, octahedral Mg is unusually high and shows no decrease with illitization in contrast to other studies of smectite illitization. (2) As smectite illitization proceeds, particle shapes undergo abrupt changes from anhedral plates to laths and then to euhedral plates and hexagons. (3) I-S three-dimensionsal structure changes from turbostratic, *cv*-smectite to $1M_d$, interstratified *cv*/*tv* I-S to $1M$, *tv*-illite to $2M_1$ illite. (4) The proposed mechanism of smectite illitization on Ponza is a multi-step model, in which I-S undergoes various dissolution and crystallization reactions. The alteration temperature provides the major control for the layer composition, polytype, cation ordering, and morphology of I-S crystallites.

ACKNOWLEDGMENTS

The authors would like to thank A. Blum, G. Christidis, and S. Guggenheim for their constructive reviews that improved the quality of this manuscript. In addition, we thank I. Steele at the University of Chicago for assistance with microprobe data, C. Demosthenous and G. Rolandi for their assistance in the field, D. Finkelstein, G. Grathoff, R.L. Hay, and R.C. Reynolds for valuable discussions, and W. Holzwarth for helping prepare figures. This work was part of RFY's Ph.D. thesis and supported by a NSF graduate student fellowship and NSF grant EAR 9417758.

REFERENCES

Ahn, J-H. and Peacor, D.R. (1986) Transmission and analytical electron microscopy of the smectite-to-illite transition. *Clays and Clay Minerals*, **34,** 165–179.

Altaner, S.P. and Ylagan, R.F. (1997) Comparison of structural models of mixed-layer illite-smectite and reaction mechanisms of smectite illitization. *Clays and Clay Minerals*, **45,** 517–533.

Altaner, S.P., Weiss, C.A., and Kirkpatrick, R.J. (1988) Evidence from ^{29}Si NMR for the structure of mixed layer illite-smectite clay minerals. *Nature*, **331,** 699–702.

Awwiller, D.N. (1993) Illite-smectite formation and potassium mass transfer during burial diagenesis of mudrocks: A study from the Texas Gulf Coast Paleocene-Eocene. *Journal of Sedimentary Petrology*, **63,** 501–512.

Barberi, F., Borsi, S., Ferrara, G., and Innocenti, F. (1967) Contributo alla conoscenza vulcanologica e magmatologica delle Isole dell'Arcipelago Pontino. *Memorie della Societa Geologica Italiana*, **6,** 581–606.

Barronnet, A. (1982) Ostwald Ripening in solutions: The case of calcite and mica. *Estudios Geologicos*, **38,** 185–198.

Baronnet, A. (1992) Polytypism and stacking disorder. In *Minerals and Reactions at the Atomic Scale: Transmission Electron Microscopy*, P.R. Buseck, ed., Mineralogical Society of America, Chelsea, Michigan, 231–288.

Baxter Grubb, S.M., Peacor, D.R., and Jiang, W-T. (1991) Transmission electron microscope observations of illite polytypism. *Clays and Clay Minerals*, **30,** 540–550.

Beccaluva, L., Brotzu, P., Macciotta, G., Morbidelli, L., Serri, G., and Traversa, G. (1989) Cainozoic tectono-magmatic evolution and inferred mantle sources in the Sardo-Tyrrhenian area. In *The Lithosphere in Italy*, A. Boriani, M. Bonafede, G.B. Piccardo, and G.B. Vai, eds., Accademia Nazionale dei Lincei, Rome, 229–248.

Bethke, C.M., Vergo, N., and Altaner, S.P. (1986) Pathways of smectite illitization. *Clays and Clay Minerals*, **34,** 125–135.

Blum, A. (1994) Determination of illite-smectite particle morphology using scanning force microscopy. In *Scanning Probe Microscopy of Clay Minerals*, K.L. Nagy and A. Blum, eds., Clay Mineral Society, Boulder, Colorado, 171–202.

Brusewitz, A. (1986) Chemical and physical properties of Paleozoic potassium bentonites from Kinnekulle, Sweden. *Clays and Clay Minerals*, **34,** 442–454.

Capaldi, G., Civetta, L., and Gillot, P.Y. (1985) Geochronology of Plio-Pleistocene volcanic rocks from southern Italy. *Rendiconti della Societa Italiana Minerologica Petrologia*, **40,** 25–44.

Carmassi, M., De Rita, D., Di Filippo, M., Funiciello, R., and Sheridan, M.F. (1983) Geology and volcanic evolution of the island of Ponza, Italy. *Geologica Roma*, **22,** 211–232.

Christidis, G.E. (1995) Mechanism of illitization of bentonites in the geothermal field of Milos Island, Greece: Evidence based on mineralogy, chemistry, particle thickness and morphology. *Clays and Clay Minerals*, **43,** 569–585.

Christidis, G. and Dunham, A.C. (1993) Compositional variations in smectites: Part I: Alteration of intermediate volcanic rocks. A case study from Milos Island, Greece. *Clay Minerals*, **28,** 255–273.

Civetta, L., Francalanci, L., Manetti, P., and Peccerillo, A. (1989) Petrological and geochemical variations across the Roman comagmatic province: Inference on magma genesis and crust-mantle evolution. In *The Lithosphere in Italy*, A. Boriani, M. Bonafede, G.B. Piccardo, and G.B. Vai, eds., Accademia Nazionale dei Lincei, Rome, 249–269.

Clauer, N., Furlan, S., and Chaudhuri, S. (1995) The illitization process in deeply buried shales of the Gulf Coast area. *Clays and Clay Minerals*, **43,** 257–259.

Dewey, J.F. (1988) Extensional collapse of orogens. *Tectonics*, **7,** 1123–1139.

Di Marco, M.J., Ferrell, R.E., and Lowe, D.R. (1989) Polytypes of 2:1 dioctahedral micas in silicified volcaniclastic sandstones, Warrawoona group, Pilbara block, western Australia. *American Journal of Science*, **289,** 649–660.

Drits, V.A. (1987) Mixed-layer minerals: Diffraction methods and structural features. In *Proceedings of the International Clay Conference, Denver, (1985),* L.G. Schultz, H. van Olphen, and F.A. Mumpton, eds., Clay Mineral Society, Bloomington, Indiana, 33–45.

Drits, V.A., Plancon, A.B., Sakharov, B.A., Besson, G., Tsipursky, S.I., and Tchoubar, C. (1984) Diffraction effects calculated for structural models of K-saturated montmorillonite containing different types of defects. *Clay Minerals*, **19,** 541–561.

Drits, V.A., Weber, F., Salyn, A.L., and Tsipursky, S.I. (1993) X-ray identification of one-layer illite varieties: Application to the study of illites around uranium deposits of Canada. *Clays and Clay Minerals*, **41,** 389–398.

Drits, V.A., Salyn, A.L., and Šucha, V. (1996) Structural transformations of interstratified illite-smectite from Dolná Ves hydrothermal deposits: Dynamics and mechanisms. *Clays and Clay Minerals*, **44,** 181–190.

Eberl, D.D. and Środoń, J. (1988) Ostwald ripening and interparticle-diffraction effects for illite crystals. *American Mineralogist*, **73,** 1335–1345.

Eberl, D.D., Środoń, J., Lee, M., Nadeau, P.H., and Northrop, H.R. (1987) Sericite from the Silverton caldera, CO: Correlation among structure, composition, origin, and particle thickness. *American Mineralogist*, **72,** 914–935.

Eberl, D.D., Środoń, J., Kralik, M., Taylor, B.E., and Peterman, Z.E. (1990) Ostwald ripening of clays and metamorphic minerals. *Science*, **248,** 474–477.

Ferrara, G. and Tonarini, S. (1985) Radiometric geochronology in Tuscany: Results and problems. *Rendiconti della Societa Italiana Minerologica Petrologia*, **40,** 111–124.

Ferrara, G., Giuliani, O., Tonarini, S., and Villa, I.M. (1988) Datability and isotopic disequilibrium in anatectic volcanites from San Vincenzo and Tolfa (Tuscany–Latium). *Rendiconti della Societa Italiana Minerologica Petrologia*, **7,** 72.

Fornaseri, M. (1985) Geochronology of volcanic rocks from Latium (Italy). *Rendiconti della Societa Italiana Minerologica Petrologia*, **40,** 73–106.

Grim, R.E. and Güven, N. (1978) *Bentonites: Geology, Mineralogy, Properties and Uses*. Elsevier, Amsterdam, 256 pp.

Güven, N and Grim, R. (1972) X-ray diffraction and electron optical studies on smectite and cristobalite associations. *Clays and Clay Minerals*, **20,** 89–92.

Hajish, A. and Chandler, G.W. (1981) An experimental investigation of high-temperature interactions between seawater and rhyolite, andesite, basalt, and peridotite. *Contributions to Mineralogy and Petrology*, **78,** 240–254.

Hawkesworth, C.J. and Vollmer, R. (1979) Crustal contamination versus enriched mantle: $^{143}Nd/^{144}Nd$ and $^{87}Sr/^{86}$ Sr evidence from the Italian volcanics. *Contributions to Mineralogy and Petrology*, **69,** 151–165.

Hower, J. (1981) Shale diagenesis. In *Clays and the Resource Geologist*, F.J. Longstaffe, ed., Mineralogical Society of Canada, 60–80.

Hunziker, J.C., Frey, M., Clauer, N., Dallmeyer, R.D., Friedrichsen, H., Flehmig, W., Hochstrasser, K., Roggwiler, P., and Schwander, H. (1986) The evolution of illite to muscovite: Mineralogical and isotopic data from the Glarus Alps, Switzerland. *Contributions to Mineralogy and Petrology*, **92,** 157–180.

Inoue, A. and Kitagawa, R. (1994) Morphological characteristics of illitic clay minerals from a hydrothermal system. *American Mineralogist*, **79,** 700–711.

Inoue, A. and Utada, M. (1983) Further investigations of a conversion series of dioctahedral mica/smectites in the Shinzan hydrothermal alteration area, northeast Japan. *Clays and Clay Minerals*, **31,** 401–412.

Inoue, A., Minato, H., and Utada, M. (1978) Mineralogical properties and occurrence of illite/montmorillonite mixed layer minerals formed from Miocene volcanic glass in Waga-Omono district. *Clay Science*, **5,** 123–136.

Inoue, A., Kohyama, N., Kitagawa, R., and Watanabe T. (1987) Chemical and morphological evidence for the conversion of smectite to illite. *Clays and Clay Minerals*, **35,** 111–120.

Inoue, A., Velde, B., Meunier, A., and Touchard, G. (1988) Mechanism of illite formation during smectite-to-illite conversion in a hydrothermal system. *American Mineralogist*, **73,** 1325–1334.

Inoue, A., Watanabe, T., Kohyama, N., and Brusewitz, A.M. (1990) Characterization of illitization of smectite in bentonite beds at Kinnekulle, Sweden. *Clays and Clay Minerals*, **38,** 241–249.

Lanson, B., Velde, B., and Meunier, A. (1998) Late-stage diagenesis of illitic clay minerals as seen by decomposition of X-ray diffraction patterns: Contrasted behaviors of sedimentary basins with different burial histories. *Clays and Clay Minerals*, **46,** 69–78.

Lee, J.H., Ahn, J-H., and Peacor, D.R. (1985) Textures in layered silicates: Progressive changes through diagenesis and low-temperature metamorphism. *Journal of Sedimentary Petrology*, **55,** 532–540.

Li, G., Peacor, D.R., and Coombs, D.S. (1997) Transformation of smectite to illite in bentonite and associated sediments from Kaka Point, New Zealand: Contrast in rate and mechanism. *Clays and Clay Minerals*, **45,** 54–67.

Lindgreen, H., Jacobsen, H., and Jakobsen, H.J. (1991) Diagenetic structural transformations in North Sea Jurassic illite-smectite. *Clays and Clay Minerals*, **39,** 54–69.

Lombardi, G. and Mattias, P. (1981) *Guidebook for the Excursions in Sardinia and Central Italy*. Association pour l'Etude des Argiles (AIPEA), Rome, 96 pp.

Lonker, S.W. and Fitz Gerald, J.D. (1990) Formation of coexisting 1*M* and 2*M* polytypes in illite from an active hydrothermal system. *American Mineralogist*, **75,** 1282–1289.

Lupino, R. (1954) Sulla bentonite dell'Isola di Ponza. *La Ricerca Scienza*, **24,** 2326–2339.

Lynch, F.L., Mack, L.E., and Land, L.S. (1997) Chemical and mineralogical burial-diagenesis of illite-smectite in shales and the origins of authigenic quartz and secondary porosity in sandstones. *Geochimica et Cosmochimica Acta*, **61,** 1995–2006.

Marino, M.C. (1992) Caratteristiche vulcanologiche e geochimiche delle Isole di Ponza e Ventotene. Degree thesis, University of Naples, Naples, Italy.

McCarty, D.K. and Reynolds, R.C. (1995) Rotationally disordered illite-smectite in Paleozoic K-bentonites. *Clays and Clay Minerals*, **43,** 271–284.

Mukhamet-Galeyev, A.P., Pokrovskiy, V.A., Zotov, A.V., Ivanov, I.P., and Samotoin N.D. (1985) Kinetics and mechanism of hydrothermal crystallation of $2M_1$ muscovite: An experimental study. *International Geological Review*, **27,** 1352–1364.

Nadeau, P.H. and Bain, D.C. (1986) Composition of some smectites and diagenetic illitic clays and implications for their origin. *Clays and Clay Minerals*, **34,** 455–464.

Nadeau, P.H., Wilson, M.J., McHardy, W.J., and Tait, J.M. (1984) Interstratified clays as fundamental particles. *Science*, **225,** 923–925.

Nadeau, P.H., Wilson, M.J., McHardy, W.J., and Tait, J.M. (1985) The conversion of smectite to illite during diagenesis: Evidence from some illitic clays from bentonites and sandstones. *Minerolgical Magazine*, **49,** 393–400.

Newmann, A.C.D. and Brown, G. (1987) The chemical constitution of clays. In *Chemistry of Clays and Clay Minerals*, A.C.D. Newmann and G. Brown, eds., Mineralogical Society, London, 1–128.

Passaglia, E., Artioli, G., Gualtieri, A., and Carnevali, R. (1995) Diagenetic mordenite from Ponza, Italy. *European Journal of Mineralogy*, **7,** 429–438.

Pearce, R.B. and Clayton, T. (1995) Tschermak substitution as an indicator of palaeotemperature in Silurian K-bentonites from the southern uplands of Scotland and northern Ireland. *Clay Minerals*, **30,** 15–25.

Peccerillo, A., Conticelli, S., and Manetti, P. (1987) Petrological characteristics and the genesis of the recent magmatism of southern Tuscany and northern Latium. *Per Mineral*, **56,** 157–172.

Pichler, H. (1965) Acid hyaloclastites. *Bulletin of Volcanology*, **28,** 293–312.

Poli, G. (1992) Geochemistry of Tuscan archipelago granitoids, central Italy: The role of hybridization processes in their genesis. *Journal of Geology*, **100,** 41–56.

Pollard, C.O. (1971) Semidisplacive mechanism for diagenetic alteration of montmorillonite layers to illite layers. *Appendix: Geological Society of America Special Paper*, **134,** 79–93.

Pozzuoli, A. (1988) Mineralogy, geochemistry, and origin of alteration products in the Pontian archipelago, Italy: I. The genesis of the Ponza bentonite. In *Proceedings of the 10th Conference on Clay Mineralogy and Petrology*. J. Konta, ed., Ostrava, Czechoslovakia, 89–98.

Pozzuoli A. (1992) Genesis and time of formation of the Ponza island bentonite (Italy). *Trends in Mineralogy*, **1,** 57–63.

Reynolds, R.C. (1980) Interstratified clay minerals. In *Chemistry of Clays and Clay Minerals*, A.C.D. Newmann and G. Brown, eds., Mineralogical Society, London, 249–303.

Reynolds, R.C. (1985) NEWMOD—A computer program for the calculation of basal diffraction intensities of mixed-layered clay minerals, R.C. Reynolds, 8 Brook Road, Hanover, New Hampshire, 24 pp.

Reynolds, R.C. (1992) X-ray diffraction studies of illite-smectite from rocks, <1 μm randomly oriented powders, and <1 μm oriented powder aggregates: The absence of laboratory-induced artifacts. *Clays and Clay Minerals*, **40,** 387–396.

Reynolds, R.C. (1993a) Three-dimensional X-ray powder diffraction from disordered illite: Simulations and interpretation of the diffraction patterns. In *Computer Applications to X-ray Powder Diffraction Analysis of Clay Minerals*, R.C. Reynolds and J.R. Walker, eds., Clay Minerals Society, Boulder, Colorado, 44–78.

Reynolds, R.C. (1993b) WILDFIRE—A Computer Program for the Calculation of Three-Dimensional Powder X-ray Diffraction Patterns for Mica Polytypes and Their Disordered Variations, R.C. Reynolds, 8 Brook Road, Hanover, New Hampshire, 66 pp.

Reynolds, R.C. and Thomson, C.H. (1993) Illite from the Potsdam sandstone of New York: A probable noncentrosymmetric mica structure. *Clays and Clay Minerals*, **41,** 66–72.

Rogers, N.W., Hawkesworth, C.J., Parker, R.J., and Marsh, J.S. (1985) The geochemistry of potassic lavas from Vulsini, central Italy and implications for mantle enrichment processes beneath the Roman region. *Contributions to Mineralogy and Petrology*, **90,** 244–257.

Savelli C. (1983) Eta' K/Ar delle principali manifestazioni riolitiche dell'isola di Ponza. *Rendiconti della Societa Italiana*, **6,** 39–42.

Savelli, C. (1987) K/Ar ages and chemical data of volcanism in the western Pontine Islands (Tyrrhenian Sea). *Bolletino della Societa Geologica Italiana*, **106,** 537–546.

Shiraki, R., Sakai, H., Endoh, M., and Kishima, N. (1987) Experimental studies on rhyolite- and andesite-seawater interactions at 300°C and 1000 bars. *Geochemical Journal*, **21,** 139–148.

Small, J.S., Hamilton, D.L., and Habesch, S. (1992a) Experimental simulation of clay precipitation within reservoir sandstones 1: Techniques and examples. *Journal of Sedimentary Petrology*, **62,** 508–519.

Small, J.S., Hamilton, D.L., and Habesch, S. (1992b) Experimental simulation of clay precipitation within reservoir sandstones 2: Mechanism of illite formation and controls on morphology. *Journal of Sedimentary Petrology*, **62,** 520–529.

Smith, J.V. and Ribbe, P.H. (1966) X-ray emission microanalysis of rock-forming minerals III. Alkali feldspars. *Journal of Geology*, **74,** 197–216.

Środoń, J. and Eberl, D.D. (1984) Illite. In *Micas*, S.W. Bailey, ed., Mineralogical Society of America, Chelsea, Michigan, 495–544.

Środoń, J., Morgan, D.J., Eslinger, E.V., Eberl, D.D., and Karlinger, M.R. (1986) Chemistry of illite-smectite and end-member illite. *Clays and Clay Minerals*, **34,** 368–378.

Środoń, J., Elsass, F., McHardy, W.J., and Morgan, D.J. (1992) Chemistry of illite-smectite inferred from TEM measurements of fundamental particles. *Clay Minerals*, **27,** 137–158.

Šucha, V., Kraus, I., Mosser, C., Hroncova, Z., Soboleva, K.A., and Siranova, V. (1992) Mixed-layer illite-smectite from the Dolna Ves hydrothermal deposit, the western Carpathians Kremnica Mts. *Geologica Carpathia*, **1,** 13–19.

Taylor, H.P. and Turi, B. (1976) High ^{18}O igneous rocks from the Tuscan magmatic province, Italy. *Contributions to Mineralogy and Petrology*, **55,** 33–54.

Taylor, H.P., Gregory, R.T., and Turi, B. (1987) $^{18}O/^{16}O$ evidence for fluid-rock interaction in the upper mantle: Data from ultramafic nodules and K-rich volcanic volcanic rocks in Italy. In *Stable Isotopes at High Temperatures*, H.C. Helgeson, ed., Mineralogical Society of America, Chelsea, Michigan, 1–37.

Tsipursky, S.I. and Drits, V.A. (1984) The distribution of octahedral cations in the 2:1 layers of dioctahedral smectites studied by oblique texture electron diffraction. *Clay Minerals*, **19,** 177–193.

Turi, B. and Taylor, H.P. (1976) Oxygen isotope studies of potassic volcanic rocks of the Roman province, central Italy. *Contributions to Mineralogy and Petrology*, **55,** 1–31.

Turi, B., Taylor, H.P., and Ferrara, G. (1991) Comparisons of $^{18}O/^{16}O$ and $^{87}Sr/^{86}Sr$ in volcanic rocks from the Pontine Islands, M. Enrici, and Campania with other areas in Italy. In *Stable Isotope Geochemistry: A Tribute to Samuel Epstein*, H.P. Taylor, J.R. O'Neil, and I.R. Kaplan, eds., The Geochemical Society, 307–324.

Velde, B. (1965) Experimental determination of muscovite polymorph stabilities. *American Mineralogist*, **50,** 436–449.

Velde, B. and Hower, J. (1963) Petrological significance of illite polymorphism in Paleozoic sedimentary rocks. *American Mineralogist*, **48,** 1239–1254.

Warshaw, C.M. (1960) Experimental studies of illite. *Clays and Clay Minerals*, **5,** 303–316.

Whitney, G. and Northrop, H.R. (1988) Experimental investigation of the smectite to illite reaction: Dual reaction

mechanisms and oxygen-isotope systematics. *American Mineralogist*, **73,** 77–90.

Whitney, G. and Velde, B. (1993) Changes in particle morphology during illitization: An experimental study. *Clays and Clay Minerals*, **41,** 209–218.

Yamagishi, H. and Dimroth, E. (1985) A comparison of Miocene and Archean rhyolite hyaloclastites: Evidence for a hot and fluid rhyolite lava flow. *Journal of Volcanology and Geothermal Research*, **23,** 337–355.

Yau, Y-C., Peacor, D.R., and McDowell, S.D. (1987) Smectite-to-illite reactions in Salton Sea shales: A transmission and analytical electron microscopy study. *Journal of Sedimentary Petrology*, **57,** 335–342.

Ylagan, R.F. (1996) Mineralogy and geochemistry associated with hydrothermal alteration of a rhyolitic hyaloclastite from Ponza island, Italy. Ph.D. thesis, University of Illinois, Urbana, Illinois, 153 pp.

Ylagan, R.F., Altaner, S.P., and Pozzuoli, A.P. (1996) Hydrothermal alteration of a rhyolitic hyaloclastite from Ponza island, Italy. *Journal of Volcanology and Geothermal Research*, **74,** 215–231.

Zielinski, R.A. (1982) The mobility of uranium and other elements during alteration of rhyolite ash to montmorillonite: A case study in the Troublesome formation, Colorado, U.S.A. *Chemical Geology*, **35,** 185–204.

E-mail of corresponding author: bob.f.ylagan@exxon.sprint.com

(Received 13 July 1998; accepted 16 June 2000; Ms. 98-093; A.E. W. Crawford Elliott)